

# Quadrupolar spin liquid, octupolar Kondo coupling and odd-frequency superconductivity in an exactly solvable model

Carlene S. de Farias,<sup>1,2</sup> Vanuilo S. de Carvalho,<sup>1</sup> Eduardo Miranda,<sup>1</sup> and Rodrigo G. Pereira<sup>2</sup>

<sup>1</sup>*Instituto de Física Gleb Wataghin, Unicamp, Campinas, SP, 13083-859, Brazil*

<sup>2</sup>*International Institute of Physics and Departamento de Física Teórica e Experimental, Universidade Federal do Rio Grande do Norte, Campus Universitário, Lagoa Nova, Natal, RN, 59078-970, Brazil*  
(Dated: June 13, 2022)

We propose an exactly solvable model on the honeycomb lattice in which  $j_{\text{eff}} = \frac{3}{2}$  local moments interact via bond-dependent quadrupole-quadrupole interactions. The model is solved using a Majorana fermion representation for multipole operators. When time reversal symmetry is explicitly broken, we obtain a gapped spin liquid characterized by three chiral edge states. We also investigate another solvable model in which the time-reversal-invariant spin liquid is coupled to conduction electrons in a superconductor. In the presence of a Kondo coupling that involves the octupole moment of the localized spins, the itinerant electrons hybridize with the emergent Majorana fermions in the spin liquid. This leads to spontaneous time reversal symmetry breaking and generates odd-frequency pairing. Our results suggest that  $j_{\text{eff}} = \frac{3}{2}$  systems with strong quadrupole-quadrupole interactions may provide a route towards non-Abelian quantum spin liquids and unconventional superconductivity.

## I. INTRODUCTION

Quantum spin liquid phases have fascinated condensed matter physicists since Anderson's proposal of resonating valence bond states [1, 2]. These phases harbor exotic properties such as spin fractionalization and long-range entanglement [3, 4]. Unlike classical magnetic phases that spontaneously break symmetries of the Hamiltonian, quantum spin liquids are not characterized by local order parameters; in fact, their study helped develop the concept of topological order [5, 6].

Kitaev's honeycomb model [7] is the best known example of an exactly solvable model with a quantum spin liquid ground state. The solution works by expressing the spin  $S = \frac{1}{2}$  operators in terms of Majorana fermions and realizing that the exact excitations correspond to deconfined Majorana fermions in the background of a static  $\mathbb{Z}_2$  gauge field. Experimentally, the bond-dependent anisotropic exchange interaction of the Kitaev model is realized in the iridates  $(\text{Na}, \text{Li})_2\text{IrO}_3$  and the ruthenium compound  $\alpha\text{-RuCl}_3$  [8–10], where it is generated via the Jackeli-Khalliulin mechanism [11, 12]. Essential ingredients for the latter are the strong spin-orbit coupling of  $4d^5$  or  $5d^5$  magnetic ions and the environment of edge-sharing octahedra formed by the ligands. The Kitaev interaction, parametrized by coupling constant  $K$ , arises as the leading term in the effective spin model for  $j_{\text{eff}} = \frac{1}{2}$  local moments. A more general model that takes into account subleading exchange paths and trigonal distortions of the octahedra must also include the Heisenberg interaction  $J$  and the anisotropic interactions denoted  $\Gamma$  and  $\Gamma'$  [13, 14]. As a matter of fact, the Kitaev model can be regarded as an exactly solvable point in the parameter space of the  $J$ - $K$ - $\Gamma$ - $\Gamma'$  model. In the iridates and  $\alpha\text{-RuCl}_3$ , the additional couplings beyond the Kitaev model are large enough that these materials fall outside the Kitaev spin liquid phase and undergo magnetic ordering transitions

at low temperatures [8–10].

In the past few years, alternative routes to Kitaev magnetism have been explored. In particular, the search has been extended to systems with more degrees of freedom, beyond the picture of  $j_{\text{eff}} = \frac{1}{2}$  moments. For instance, materials with  $4d^1$  or  $5d^1$  configuration are described by effective models with  $j_{\text{eff}} = \frac{3}{2}$  moments, which can be represented by pseudospin and pseudo-orbital degrees of freedom [15–18]. The higher value of  $j_{\text{eff}}$  allows for multipolar interactions which can promote hidden multipolar orders or even quantum spin-orbital liquid phases [19–23]. Multipolar interactions also play an important role in rare-earth systems [24–28], where electrons in the  $f$ -shell are much more localized and have stronger spin-orbit coupling than  $d$  electrons in transition metal compounds. Indeed, rare-earth magnets analogous to  $j_{\text{eff}} = \frac{1}{2}$  Kitaev materials have been proposed recently [29–31]. The spin- $S$  Kitaev model with  $S > \frac{1}{2}$ , generated microscopically by Hund's coupling in the transition metal and strong spin-orbit coupling in the ligands, has also attracted considerable attention [32–37]. Unlike the original  $S = \frac{1}{2}$  Kitaev model [7], however, these higher spin models are not integrable in general, and the characterization of putative quantum spin liquid phases needs to rely on numerics or analytical mean-field approximations.

In this paper, we propose an exactly solvable  $j_{\text{eff}} = \frac{3}{2}$  model on the honeycomb lattice with a spin-orbital liquid ground state and Majorana fermion excitations. In contrast with previous generalizations of the Kitaev model to higher-dimensional local Hilbert spaces [38–41], our analysis is guided by the symmetries of  $j_{\text{eff}} = \frac{3}{2}$  states in an octahedral crystal field, such that the pseudo-orbital degree of freedom transforms as in a  $120^\circ$  quantum compass model [17, 42]. This makes our model an exactly solvable point in the parameter space of the more general model for  $j_{\text{eff}} = \frac{3}{2}$  systems. It may be relevant to  $4d^1$  or  $5d^1$  materials as well as for rare-earth systems with a

$\Gamma_8$  quartet ground state [25, 43]. Our spin-orbital Hamiltonian can be interpreted as a quadrupole-quadrupole interaction, which in fact appears as a symmetry-allowed term in the model for  $j_{\text{eff}} = \frac{3}{2}$  honeycomb systems including the effects of Hund's coupling [21]. We also consider a single-ion anisotropy term that lowers the point group symmetry and leads to a nonzero expectation value of the local quadrupole moment. Upon breaking time reversal symmetry, we obtain fully gapped spin-orbital excitations in the bulk, but three gapless modes on the edge.

Furthermore, we investigate the coupling of this “quadrupolar spin liquid” to itinerant electrons, as illustrated in Fig. 1. This part is motivated by recent studies of the Kondo-Kitaev model within mean-field approximations [44, 45] and by *ab initio* calculations of  $\alpha$ -RuCl<sub>3</sub>/graphene heterostructures [46], which suggest that the Kondo coupling between a Fermi liquid and a Kitaev spin liquid can give rise to exotic superconductivity. Again we choose the interactions so that the total Hamiltonian is exactly solvable in terms of free Majorana fermions and conserved  $\mathbb{Z}_2$  bond variables. This requires the decoupled electronic system to be a superconductor that breaks inversion and SU(2) spin rotational symmetry, but preserves time reversal symmetry. The itinerant electrons and  $j_{\text{eff}} = \frac{3}{2}$  local moments interact via an octupolar Kondo coupling, analogous to the coupling studied in the context of heavy-fermion systems where the magnetic ions form non-Kramers doublets [47, 48]. We find that the hybridization between Majorana fermions in the spin liquid and in the superconductor leads to *spontaneous* breaking of time reversal symmetry. Within the exactly solvable model, the ground state is degenerate between the choices of uniform (“ferro”) or staggered (“antiferro”) hybridization order parameters. In both cases, the effective action for the electrons in the superconductor contains odd-frequency pairing [49–53]. We then analyze the effects of weak integrability-breaking perturbations that lift this degeneracy, and obtain either a gapped superconductor with chiral edge states or a gapless superconductor with a Bogoliubov Fermi surface [54] and antichiral edge states [55].

The paper is organized as follows. First, in Sec. II, we introduce the exactly solvable model with quadrupole-quadrupole interactions between local moments. In Sec. III, we consider the full model with the octupolar Kondo coupling between the spin liquid and the superconductor. We discuss properties of the spectrum and the spontaneous time reversal symmetry breaking in the coupled system. In Sec. IV, we calculate the effective action for the electrons in the superconductor after exactly integrating out the Majorana fermions associated with the local moments. In Sec. V, we analyze the effects of perturbations to the exactly solvable model. Finally, we present our conclusions in Sec. VI.

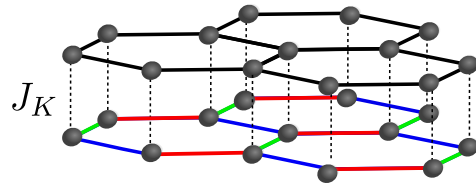


FIG. 1. Schematic representation of the honeycomb lattice containing the spin liquid (lower plane) and the itinerant electron (upper plane) degrees of freedom. The  $j_{\text{eff}} = \frac{3}{2}$  local moments in the spin liquid interact via Kitaev-like quadrupole-quadrupole interactions  $K_\gamma$ , with  $\gamma = x, y, z$  labeling the different nearest-neighbor bonds indicated by the colors red, blue and green, respectively. The conduction electrons are described by nearest-neighbor and next-nearest-neighbor couplings which include hopping and pairing amplitudes. The two subsystems interact via an octupolar Kondo coupling  $J_K$ .

## II. EXACTLY SOLVABLE QUADRUPOLAR SPIN LIQUID MODEL

### A. Symmetry considerations

Consider local moments with effective total angular momentum  $j_{\text{eff}} = \frac{3}{2}$ . For concreteness, we can think of transition metal ions with a  $4d^1$  or  $5d^1$  configuration subject to a strong crystal field of ligand octahedra and to strong spin-orbit coupling. In this case, the single electron in the open  $d$  shell occupies the threefold degenerate  $t_{2g}$  orbitals with effective orbital angular momentum  $l_{\text{eff}} = 1$ . The spin-orbit coupling splits the energy levels into a higher-energy  $j_{\text{eff}} = \frac{1}{2}$  doublet and the low-lying  $j_{\text{eff}} = \frac{3}{2}$  quadruplet [9]. Alternatively, we may consider rare earth ions which have a quartet ground state in an octahedral crystal field [25, 26].

The local Hilbert space is spanned by the four eigenstates of the  $J^z$  operator,  $J^z|m_J\rangle = m_J|m_J\rangle$ , with  $m_J = \pm\frac{1}{2}, \pm\frac{3}{2}$ . These states transform under rotations as the  $\Gamma_8$  representation of the octahedral double group [43]. The operators acting in the local Hilbert space can be organized into dipole, quadrupole and octupole moments [25, 27] as shown in Table I. While the dipole and octupole moments involve odd powers of components of  $\mathbf{J}$  and change sign under time reversal, the quadrupole moments contain even powers and are time-reversal invariant.

We rewrite the eigenstates of  $J^z$  in terms of two pseudospin-1/2 quantum numbers in the form  $|s^z, \tau^z\rangle$  [16, 25], identifying

$$\begin{aligned} |m_J = \frac{3}{2}\rangle &= |s^z = -\frac{1}{2}, \tau^z = \frac{1}{2}\rangle \equiv |-+\rangle, \\ |m_J = \frac{1}{2}\rangle &= -|s^z = \frac{1}{2}, \tau^z = -\frac{1}{2}\rangle \equiv |-+-\rangle, \\ |m_J = -\frac{1}{2}\rangle &= |s^z = -\frac{1}{2}, \tau^z = -\frac{1}{2}\rangle \equiv |--\rangle, \\ |m_J = -\frac{3}{2}\rangle &= -|s^z = \frac{1}{2}, \tau^z = \frac{1}{2}\rangle \equiv |-++\rangle. \end{aligned} \quad (1)$$

We refer to  $s^z$  and  $\tau^z$  as the pseudospin and pseudo-orbital quantum numbers, respectively. The operators  $s$

TABLE I. Local operators acting on  $j_{\text{eff}} = \frac{3}{2}$  states. Overlines indicate the symmetrization with respect to permutations of the indices, e.g.,  $\overline{J^x(J^y)^2} = J^x(J^y)^2 + J^y J^x J^y + (J^y)^2 J^x$ . Here  $\mathbf{u}^\gamma$  and  $\mathbf{v}^\gamma$  are unit vectors in the  $xz$  plane given by  $\mathbf{u}^x = -\frac{1}{2}\hat{\mathbf{z}} + \frac{\sqrt{3}}{2}\hat{\mathbf{x}}$ ,  $\mathbf{u}^y = -\frac{1}{2}\hat{\mathbf{z}} - \frac{\sqrt{3}}{2}\hat{\mathbf{x}}$ ,  $\mathbf{u}^z = \hat{\mathbf{z}}$ ,  $\mathbf{v}^x = -\frac{\sqrt{3}}{2}\hat{\mathbf{z}} - \frac{1}{2}\hat{\mathbf{x}}$ ,  $\mathbf{v}^y = \frac{\sqrt{3}}{2}\hat{\mathbf{z}} - \frac{1}{2}\hat{\mathbf{x}}$ ,  $\mathbf{v}^z = \hat{\mathbf{x}}$ . Adapted from Refs. [17, 25].

Moment	Symmetry	Operators	$\mathbf{s}, \boldsymbol{\tau}$ representation	Majorana representation
Dipole	$\Gamma_4$	$J^x$	$-s^x(1 + 4\mathbf{u}^x \cdot \boldsymbol{\tau})$	$\frac{i}{2}\eta^y\eta^z - 2i\eta^x\left(-\frac{1}{2}\theta^z + \frac{\sqrt{3}}{2}\theta^x\right)$
		$J^y$	$-s^y(1 + 4\mathbf{u}^y \cdot \boldsymbol{\tau})$	$\frac{i}{2}\eta^z\eta^x - 2i\eta^y\left(-\frac{1}{2}\theta^z - \frac{\sqrt{3}}{2}\theta^x\right)$
		$J^z$	$-s^z(1 + 4\mathbf{u}^z \cdot \boldsymbol{\tau})$	$\frac{i}{2}\eta^x\eta^y - 2i\eta^z\theta^z$
Quadrupole	$\Gamma_3$	$O^{3z^2-r^2} = \frac{1}{3}[3(J^z)^2 - \mathbf{J}^2]$	$2\tau^z$	$-i\theta^x\theta^y$
		$O^{x^2-y^2} = \frac{1}{\sqrt{3}}[(J^x)^2 - (J^y)^2]$	$2\tau^x$	$-i\theta^y\theta^z$
	$\Gamma_5$	$O^{xy} = \frac{1}{\sqrt{3}}\overline{J^x J^y}$	$-4s^z\tau^y$	$i\eta^z\theta^y$
		$O^{yz} = \frac{1}{\sqrt{3}}\overline{J^y J^z}$	$-4s^x\tau^y$	$i\eta^x\theta^y$
		$O^{zx} = \frac{1}{\sqrt{3}}\overline{J^x J^z}$	$-4s^y\tau^y$	$i\eta^y\theta^y$
Octupole	$\Gamma_2$	$T^{xyz} = \frac{2}{3\sqrt{3}}\overline{J^x J^y J^z}$	$2\tau^y$	$-i\theta^z\theta^x$
	$\Gamma_4$	$\frac{2}{3}(J^x)^3 - \frac{1}{3}(\overline{J^x(J^y)^2} + \overline{(J^z)^2 J^x})$	$-2s^x(1 - \mathbf{u}^x \cdot \boldsymbol{\tau})$	$i\eta^y\eta^z + \frac{i}{2}\eta^x\left(-\frac{1}{2}\theta^z + \frac{\sqrt{3}}{2}\theta^x\right)$
		$\frac{2}{3}(J^y)^3 - \frac{1}{3}(\overline{J^y(J^z)^2} + \overline{(J^x)^2 J^y})$	$-2s^y(1 - \mathbf{u}^y \cdot \boldsymbol{\tau})$	$i\eta^z\eta^x + \frac{i}{2}\eta^y\left(-\frac{1}{2}\theta^z - \frac{\sqrt{3}}{2}\theta^x\right)$
		$\frac{2}{3}(J^z)^3 - \frac{1}{3}(\overline{J^z(J^x)^2} + \overline{(J^y)^2 J^z})$	$-2s^z(1 - \mathbf{u}^z \cdot \boldsymbol{\tau})$	$i\eta^x\eta^y + \frac{i}{2}\eta^z\theta^z$
	$\Gamma_5$	$\frac{2}{3\sqrt{3}}[\overline{J^x(J^y)^2} - \overline{(J^z)^2 J^x}]$	$-4s^x\mathbf{v}^x \cdot \boldsymbol{\tau}$	$-i\eta^x\left(-\frac{1}{2}\theta^x - \frac{\sqrt{3}}{2}\theta^z\right)$
		$\frac{2}{3\sqrt{3}}[\overline{J^y(J^z)^2} - \overline{(J^x)^2 J^y}]$	$-4s^y\mathbf{v}^y \cdot \boldsymbol{\tau}$	$-i\eta^y\left(-\frac{1}{2}\theta^x + \frac{\sqrt{3}}{2}\theta^z\right)$
		$\frac{2}{3\sqrt{3}}[\overline{J^z(J^x)^2} - \overline{(J^y)^2 J^z}]$	$-4s^z\mathbf{v}^z \cdot \boldsymbol{\tau}$	$-i\eta^z\theta^x$

and  $\boldsymbol{\tau}$  acting on the corresponding degrees of freedom obey the algebra  $[s^\alpha, s^\beta] = i\epsilon^{\alpha\beta\gamma}s^\gamma$ ,  $[\tau^\alpha, \tau^\beta] = i\epsilon^{\alpha\beta\gamma}\tau^\gamma$ , and  $[s^\alpha, \tau^\beta] = 0$ . In this notation, the time reversal operator is written as  $T = -2is^y\mathcal{K}$ , where  $\mathcal{K}$  denotes complex conjugation. Thus, two states with the same  $\tau^z$  eigenvalue form a Kramers pair. States in a non-Kramers pair, having the same  $s^z$  but different  $\tau^z$ , are associated with different electronic density profiles [17]. The pseudospin and pseudo-orbital operators transform under time reversal as follows:

$$\begin{aligned} T(s^x, s^y, s^z)T^{-1} &= (-s^x, -s^y, -s^z), \\ T(\tau^x, \tau^y, \tau^z)T^{-1} &= (\tau^x, -\tau^y, \tau^z). \end{aligned} \quad (2)$$

The representation of the multipole operators in terms of  $\mathbf{s}$  and  $\boldsymbol{\tau}$  is shown in Table I. We note in particular the transformation of  $\mathbf{s}$  and  $\boldsymbol{\tau}$  under a  $C_3$  rotation around the [111] axis:

$$\begin{aligned} C_3(s^x, s^y, s^z)C_3^{-1} &= (s^y, s^z, s^x), \\ C_3(\tau^x, \tau^z)C_3^{-1} &= \left(\frac{-\tau^x - \sqrt{3}\tau^z}{2}, \frac{-\tau^z + \sqrt{3}\tau^x}{2}\right), \\ C_3\tau^yC_3^{-1} &= \tau^y. \end{aligned} \quad (3)$$

Importantly, the  $\tau^y$  operator is invariant under all rotations of the octahedral group, but changes sign under time reversal. It corresponds to the octupole moment  $T^{xyz} \propto \overline{J^x J^y J^z}$ , where the overline indicates a sum over permutations of the indices, see Table I. By contrast,  $\tau^x$  and  $\tau^z$  are associated with quadrupole moments, and  $C_3$  rotations act as 120° rotations of  $(\tau^z, \tau^x)$ .

## B. Time-reversal-invariant spin model

We begin with the model

$$H_s = \sum_{\gamma=x,y,z} \sum_{\langle ij \rangle_\gamma} K_\gamma O_i^{\alpha\beta} O_j^{\alpha\beta} - \lambda \sum_j O_j^{3z^2-r^2}, \quad (4)$$

where  $\langle ij \rangle_\gamma$  labels a nearest-neighbor bond along the  $\gamma$  direction, see Fig. 1, and  $O_j^{3z^2-r^2}$  and  $O_j^{\alpha\beta}$  [with  $(\alpha, \beta, \gamma)$  a cyclic permutation of  $(x, y, z)$ ] are quadrupole operators defined in Table I. The first term amounts to a quadrupole-quadrupole interaction often invoked in models for  $f$ -electron systems, where it stems from electrostatic or phonon-mediated interactions [24, 25, 43, 56]. In  $4d^1/5d^1$  systems, this interaction can also be generated by the coupling  $(L_i^\alpha L_i^\beta + L_i^\beta L_i^\alpha)(L_j^\alpha L_j^\beta + L_j^\beta L_j^\alpha)$  [57], where  $\mathbf{L}_i$  is the  $l_{\text{eff}} = 1$  orbital angular momentum operator of the  $t_{2g}$  states, upon projection onto the  $j_{\text{eff}} = \frac{3}{2}$  multiplet. In fact, the isotropic quadrupole-quadrupole interaction, with  $K_x = K_y = K_z$ , appears in the effective spin model for  $j_{\text{eff}} = \frac{3}{2}$  systems on tricoordinated lattices with edge-sharing octahedra [21]. The  $\lambda$  term in Eq. (4) breaks the  $C_3$  rotational symmetry even in the isotropic case. This single-ion anisotropy term can be associated with a distortion of the local octahedral environment, which lifts the degeneracy between non-Kramers pairs [15].

To see why model (4) is exactly solvable, we introduce a Majorana fermion representation for spin 3/2 [19, 38]. In terms of pseudospin and pseudo-orbital operators, we

write

$$\begin{aligned} s_j^\gamma &= -\frac{i}{4}\epsilon^{\alpha\beta\gamma}\eta_j^\alpha\eta_j^\beta, \\ \tau_j^\gamma &= -\frac{i}{4}\epsilon^{\alpha\beta\gamma}\theta_j^\alpha\theta_j^\beta, \end{aligned} \quad (5)$$

where  $\eta_j^\alpha$  and  $\theta_j^\alpha$  are Majorana fermion operators that satisfy the anticommutation relations  $\{\eta_j^\alpha, \eta_l^\beta\} = \{\theta_j^\alpha, \theta_l^\beta\} = 2\delta_{jl}\delta^{\alpha\beta}$  and  $\{\eta_j^\alpha, \theta_l^\beta\} = 0$ . Similarly to the original spin-1/2 Kitaev model [7], this Majorana fermion representation brings about a  $\mathbb{Z}_2$  gauge structure, since physical observables are invariant under  $(\eta_j^\alpha, \theta_j^\alpha) \mapsto (-\eta_j^\alpha, -\theta_j^\alpha)$ . This gauge redundancy enlarges the Hilbert space. To restrict states to the physical Hilbert space, we must impose the local constraint

$$i\eta_j^x\eta_j^y\eta_j^z\theta_j^x\theta_j^y\theta_j^z = 1 \quad \forall j. \quad (6)$$

The multipole operators are rewritten in terms of Majorana fermions as given in Table I. In this representation, time reversal symmetry is implemented as complex conjugation,  $TiT^{-1} = -i$ , combined with

$$T\theta_j^yT^{-1} = -\theta_j^y, \quad (7)$$

leaving the other Majorana fermions invariant; see Appendix A. The  $C_3$  rotation acts as a cyclic permutation of  $(\eta^x, \eta^y, \eta^z)$  and as a  $120^\circ$  rotation  $(\theta^z, \theta^x) \mapsto (-\frac{1}{2}\theta^z + \frac{\sqrt{3}}{2}\theta^x, -\frac{1}{2}\theta^x - \frac{\sqrt{3}}{2}\theta^z)$ , analogous to Eq. (3). Essentially, the “scalar” Majorana fermion  $\theta^y$  inherits the symmetry properties of the  $\tau^y$  operator.

We rewrite the Hamiltonian Eq. (4) in terms of Majorana fermions according to Table I and obtain

$$H_s = i \sum_\gamma \sum_{\langle jl \rangle_\gamma} K_\gamma \hat{u}_{\langle jl \rangle_\gamma} \theta_j^y \theta_l^y + i\lambda \sum_j \theta_j^x \theta_j^y, \quad (8)$$

where  $\hat{u}_{\langle jl \rangle_\gamma} = -i\eta_j^\gamma\eta_l^\gamma$  are antisymmetric  $\mathbb{Z}_2$  bond operators, obeying  $(\hat{u}_{\langle jl \rangle_\gamma})^2 = 1$  and  $\hat{u}_{\langle jl \rangle_\gamma} = -\hat{u}_{\langle lj \rangle_\gamma}$ , which commute with one another and with  $H_s$ . Once we fix the values of the conserved  $\hat{u}_{\langle jl \rangle_\gamma} = \pm 1$ , the Hamiltonian becomes quadratic in the remaining Majorana fermions. The ground state is in the sector with zero  $\mathbb{Z}_2$  flux [58], defined as the product of  $\hat{u}_{\langle jl \rangle_\gamma}$  around each hexagon. We then set  $\hat{u}_{\langle jl \rangle_\gamma} = 1$  for all sites  $j$  in sublattice A and  $l$  the corresponding nearest neighbors in sublattice B. The resulting Hamiltonian for  $\theta^x$  and  $\theta^y$  is translationally invariant and can be diagonalized by a Fourier transform. Here we use the notation  $\theta_j^\gamma \equiv \theta_b^\gamma(\mathbf{R})$ , where  $\mathbf{R}$  is the position of the unit cell and  $b \in \{A, B\}$  is a sublattice index. We can then write

$$\theta_j^\gamma = \sqrt{\frac{2}{N}} \sum_{\mathbf{k} \in \frac{1}{2}\text{BZ}} [e^{i\mathbf{k} \cdot \mathbf{R}} \theta_b^\gamma(\mathbf{k}) + e^{-i\mathbf{k} \cdot \mathbf{R}} \theta_b^\gamma(-\mathbf{k})], \quad (9)$$

where the fermion operators in momentum space obey  $\theta_b^\gamma(-\mathbf{k}) = [\theta_b^\gamma(\mathbf{k})]^\dagger$ , and the summation runs over half of

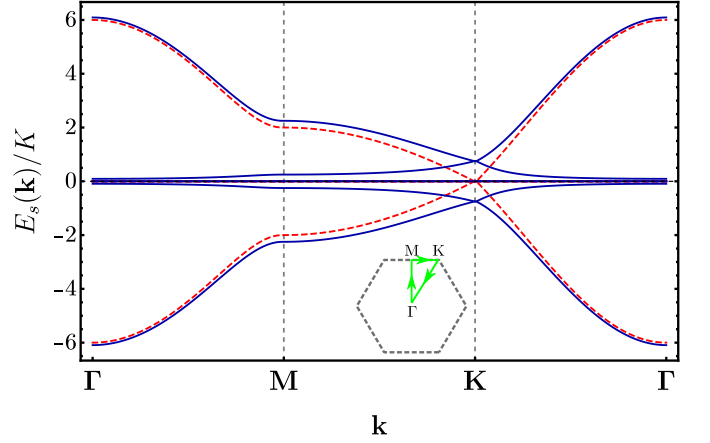


FIG. 2. Dispersion relation of the  $\theta$  Majorana fermions in the quadrupolar spin liquid along the high symmetry directions on the first Brillouin zone. Here we consider isotropic interactions,  $K_\gamma = K$ , and two values of the single-ion anisotropy parameter:  $\lambda = 0$  (dashed line) and  $\lambda/K = 0.75$  (solid line).

the Brillouin zone. We find the dispersion relations

$$E_s(\mathbf{k}) = \pm \frac{1}{\sqrt{2}} \sqrt{|g(\mathbf{k})|^2 + 2\lambda^2 \pm |g(\mathbf{k})| \sqrt{|g(\mathbf{k})|^2 + 4\lambda^2}}, \quad (10)$$

where  $g(\mathbf{k}) = K_x e^{i\mathbf{k} \cdot \mathbf{n}_1} + K_y e^{i\mathbf{k} \cdot \mathbf{n}_2} + K_z$ . Here,  $\mathbf{n}_1 = \frac{\sqrt{3}a}{2}(1, \sqrt{3})$  and  $\mathbf{n}_2 = \frac{\sqrt{3}a}{2}(-1, \sqrt{3})$  are the primitive lattice vectors in the  $xy$  plane and we set  $a = 1$ .

Having been absorbed into the bond operators, the  $\eta^\gamma$  Majorana fermions are gapped out since it costs a finite energy to create  $\mathbb{Z}_2$  vortices [7]. Figure 2 shows the dispersion relations for  $\theta$  fermions given by Eq. (10). Hereafter we focus on isotropic interactions,  $K_\gamma = K$ . Note that for  $\lambda = 0$  we have two flavors of Majorana fermions,  $\theta^x$  and  $\theta^z$ , which do not appear in the Hamiltonian. In terms of  $\tau$  operators, we have a local  $U(1)$  symmetry,  $[\tau_j^y, H_s] = 0$  for  $\lambda = 0$ . In this case, the  $\theta^y$  mode displays a gapless Dirac dispersion at the K point of the Brillouin zone, whereas  $\theta^x$  and  $\theta^z$  modes give rise to zero energy flat bands, see Fig. (2). At each site,  $\theta_j^x$  and  $\theta_j^z$  can be combined into a single complex fermion which commutes with  $H_s$ , which implies that the ground state degeneracy increases exponentially with system size.

For  $\lambda \neq 0$ , an energy gap opens up for the modes coming from the hybridization of  $\theta^x$  and  $\theta^y$ , see Fig. 2. The anisotropy associated with  $\lambda$  lowers the ground state energy and gaps out the excitations created by the pseudo-orbital operator  $\tau$ . However, the  $\theta^z$  Majorana fermions still commutes with  $H_s$ . As a consequence, the ground state of the quadrupolar spin liquid is highly degenerate even for  $\lambda \neq 0$ . In Sec. III we will couple the Hamiltonian in Eq. (4) to conduction electrons in a superconductor. We shall see that this coupling generates a dispersion for all modes and removes the exponential degeneracy in the ground state of the total system. Alternatively, we can obtain an exactly solvable spin model with a unique ground state by breaking time reversal symmetry, as we



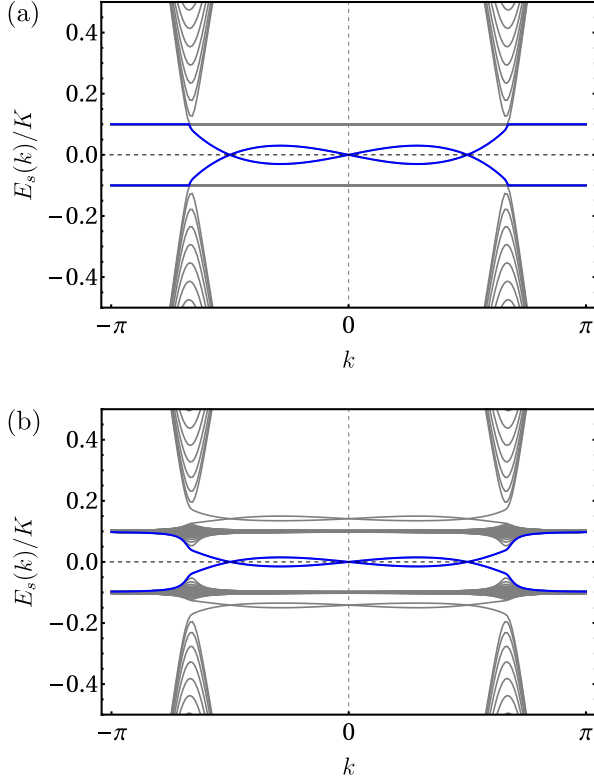


FIG. 3. Band structure of the gapped spin liquid with broken time reversal symmetry on a strip with zigzag edges and width  $W = 100$  unit cells. Here we set  $\kappa = \kappa' = 0.05K$  and consider two values of  $\lambda$ : (a)  $\lambda = 0$ ; (b)  $\lambda = 0.1K$ . In both cases, the dispersion of the edge mode crosses zero energy at three points in the projection of the Brillouin zone.

shall discuss in the next subsection.

### C. Breaking time reversal symmetry

In analogy with the Kitaev model in the presence of a magnetic field [7], we now investigate the effects of time reversal symmetry breaking in the quadrupolar spin liquid. We break time reversal while preserving the integrability of the model by adding to the Hamiltonian in Eq. (4) the following interactions:

$$\delta H_s = \kappa \sum_{\langle ij \rangle_\alpha \langle jk \rangle_\beta} O_i^{\beta\gamma} s_j^\gamma O_k^{\alpha\gamma} - \kappa' \sum_j T_j^{xyz}. \quad (11)$$

Using the Majorana fermion representation, we obtain

$$\delta H_s = i\kappa \sum_{\langle ij \rangle_\alpha \langle jk \rangle_\beta} \hat{u}_{\langle ij \rangle_\alpha} \hat{u}_{\langle jk \rangle_\beta} \theta_i^y \theta_k^y + i\kappa' \sum_j \theta_j^z \theta_j^x. \quad (12)$$

We can then fix the values of the bond variables as discussed in Sec. II B and obtain a quadratic Hamiltonian  $H_s + \delta H_s$  which involves all three  $\theta^\gamma$  Majorana fermions.

In particular, for the isotropic case  $\lambda = 0$ , the Majorana fermions  $\theta^x$  and  $\theta^z$  are decoupled from  $\theta^y$ . The

ground state in this case is an eigenstate of the local pseudo-orbital operators  $\tau_j^y$  with eigenvalue  $\tau_j^y = \frac{1}{2}$  for  $\kappa' > 0$ . The  $\kappa$  term gaps out the dispersion of the  $\theta^y$  Majorana fermions. Similarly to the Kitaev model [7], we expect this gapped spin liquid to be a topological phase. To check this, we have computed the energy spectrum of the model on a strip geometry with open boundary conditions in the  $y$  direction. In Fig. 3, we see that the spectrum contains three chiral Majorana edge modes, equivalent to a topological superconductor with Chern number  $C = \pm 3$ . This result is consistent with a recent conjecture for spin- $S$  Kitaev spin liquids [37].

We also note that for  $\lambda \neq 0$  the eigenstates of the Hamiltonian are no longer eigenstates of  $\tau_j^y$ . In this case, the coupling of  $\theta^{x,z}$  to  $\theta^y$  turns the dispersionless modes seen in Fig. 3(a) into a band of mobile pseudo-orbital excitations as shown in Fig. 3(b).

## III. COUPLING THE SPIN LIQUID TO A SUPERCONDUCTOR

We now turn to the Hamiltonian

$$H = H_s + H_c + H_K. \quad (13)$$

Here,  $H_s$  describes the quadrupolar spin liquid in Eq. (4), and we shall assume  $\lambda \neq 0$ . The new terms,  $H_c$  and  $H_K$ , describe, respectively, the conduction electrons in the superconductor and the Kondo coupling between electrons and  $j_{\text{eff}} = \frac{3}{2}$  local moments. Our goal in this section is to write down  $H_c$  and  $H_K$  that produce an exactly solvable model without any zero-energy flat bands. We shall see that the Kondo coupling gives rise to time-reversal-symmetry-breaking superconductivity.

### A. Time-reversal-invariant superconductor

The following Bogoliubov-de-Gennes Hamiltonian describes the itinerant electron system:

$$H_c = i \sum_{\langle jl \rangle} \Psi_j^\dagger [t_{jl}(\sigma^x \rho^z + \sigma^z \rho^x) + w_{jl}(\sigma^z \rho^z - \sigma^x \rho^x)] \Psi_l + i \sum_{\langle \langle jl \rangle \rangle} t'_{jl} \Psi_j^\dagger (\sigma^x \rho^z + \sigma^z \rho^x) \Psi_l. \quad (14)$$

The operator  $\Psi_j$  refers to the Balian-Werthamer spinor of the conduction electrons:

$$\Psi_j = \begin{pmatrix} \psi_j \\ -i\sigma^y(\psi_j^\dagger)^T \end{pmatrix}, \quad (15)$$

where  $\psi_j = (\psi_{j\uparrow}, \psi_{j\downarrow})^T$ . The Pauli matrices  $\sigma^\alpha$  and  $\rho^\alpha$  act in spin space and Nambu space, respectively. The parameters  $t_{jl} = -t_{lj}$ ,  $w_{jl} = -w_{lj}$  and  $t'_{jl} = -t'_{lj}$  are defined according to the orientation of nearest- and next-nearest-neighbor bonds, as illustrated in Fig. 4:  $t_{jl} = t$ ,

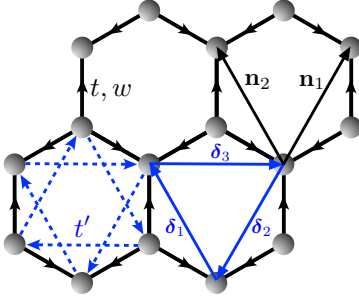


FIG. 4. Couplings in the Hamiltonian for itinerant electrons. Nearest-neighbor bonds with couplings  $t$  and  $w$  are oriented from the A to the B sublattice. Next-nearest-neighbor bonds with coupling  $t'$  are oriented as indicated by the blue dashed arrows.

$w_{jl} = w$  and  $t'_{jl} = t'$  if the corresponding arrow points from  $l$  to  $j$ , and the opposite sign if the arrow points from  $j$  to  $l$ . The Hamiltonian in Eq. (14) is invariant under time reversal,  $TiT^{-1} = -i$ ,  $T\Psi_j T^{-1} = -i\sigma^y \Psi_j$ , but breaks reflection and spin-rotational symmetries. Note that  $t$  and  $w$  alone break the sublattice inversion symmetry P:  $t_{jl} \mapsto t_{lj}$ ,  $w_{jl} \mapsto w_{lj}$ , but a nonzero next-nearest-neighbor coupling  $t'$  is required to break the inversion-like symmetry

$$\begin{aligned} P' : t_{jl} &\mapsto t_{lj}, \quad w_{jl} \mapsto w_{lj}, \quad t'_{jl} \mapsto t'_{lj}, \\ P'\Psi_j(P')^{-1} &= \begin{cases} \Psi_j & \text{if } j \in \text{sublattice A,} \\ -\Psi_j & \text{if } j \in \text{sublattice B.} \end{cases} \end{aligned} \quad (16)$$

It is convenient to use the electron operators  $\psi_{j\uparrow}$  and  $\psi_{j\downarrow}$  to define four Majorana fermions by [52]

$$\Psi_j = \frac{1}{2} \begin{pmatrix} \mathbb{1}_2 & i\mathbb{1}_2 \\ -i\sigma^y & -\sigma^y \end{pmatrix} \zeta_j, \quad (17)$$

where  $\mathbb{1}_2$  is the  $2 \times 2$  identity matrix and  $\zeta_j = (\zeta_j^1, \zeta_j^2, \zeta_j^3, \zeta_j^4)^T$ , with  $\zeta_j^\mu$  obeying  $\{\zeta_j^\mu, \zeta_l^\nu\} = 2\delta_{jl}\delta^{\mu\nu}$ . More explicitly, we have

$$\begin{aligned} \zeta_j^1 &= \psi_{j\uparrow} + \psi_{j\uparrow}^\dagger, \\ \zeta_j^2 &= \psi_{j\downarrow} + \psi_{j\downarrow}^\dagger, \\ \zeta_j^3 &= -i(\psi_{j\uparrow} - \psi_{j\uparrow}^\dagger), \\ \zeta_j^4 &= -i(\psi_{j\downarrow} - \psi_{j\downarrow}^\dagger). \end{aligned} \quad (18)$$

Time reversal acts on these Majorana fermions as

$$T : \zeta_j^1 \mapsto \zeta_j^2, \quad \zeta_j^2 \mapsto -\zeta_j^1, \quad \zeta_j^3 \mapsto \zeta_j^4, \quad \zeta_j^4 \mapsto -\zeta_j^3. \quad (19)$$

The Hamiltonian for the itinerant electrons can then be written as

$$\begin{aligned} H_c &= i \sum_{\langle jl \rangle} [t_{jl}(\zeta_j^3 \zeta_l^4 + \zeta_j^4 \zeta_l^3) + w_{jl}(\zeta_j^3 \zeta_l^3 - \zeta_j^4 \zeta_l^4)] \\ &\quad + i \sum_{\langle\langle jl \rangle\rangle} t'_{jl}(\zeta_j^3 \zeta_l^4 + \zeta_j^4 \zeta_l^3). \end{aligned} \quad (20)$$

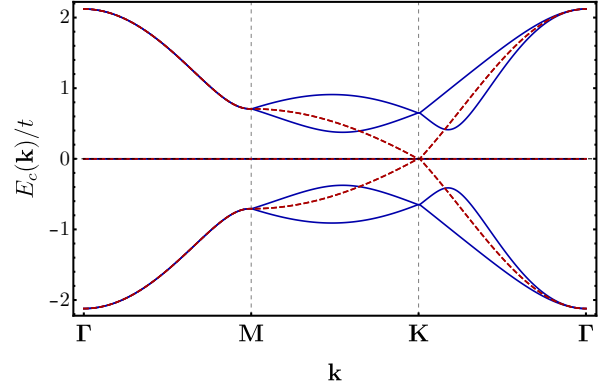


FIG. 5. Dispersion relation of itinerant electrons described by  $H_c$  in Eq. (14). Here we set  $t = w$  and consider two values of the next-nearest-neighbor coupling:  $t' = 0$  (dashed line) and  $t' = t/2$  (solid line). The zero-energy flat bands are related to the  $\zeta^1$  and  $\zeta^2$  modes.

In this form, it is clear that there are two Majorana fermions at each site,  $\zeta_j^1$  and  $\zeta_j^2$ , which commute with  $H_c$ . We have defined the conduction electron Hamiltonian this way so that we can later hybridize these zero-energy Majorana modes with the Majorana fermions in the quadrupolar spin liquid when we turn on the Kondo coupling.

We can diagonalize  $H_c$  by taking the Fourier transform of the fermion operators. We obtain the dispersion relations

$$\begin{aligned} E_c(\mathbf{k}) &= \pm [(t^2 + w^2)|f(\mathbf{k})|^2 + \Delta_0^2(\mathbf{k}) \\ &\quad \pm 2w|\Delta_0(\mathbf{k})f(\mathbf{k})|]^{1/2}, \end{aligned} \quad (21)$$

where we define the functions  $f(\mathbf{k}) = e^{i\mathbf{k} \cdot \mathbf{n}_1} + e^{i\mathbf{k} \cdot \mathbf{n}_2} + 1$  and  $\Delta_0(\mathbf{k}) = -2t' \sum_{\gamma=1}^3 \sin(\mathbf{k} \cdot \boldsymbol{\delta}_\gamma)$ , with  $\boldsymbol{\delta}_1 = \mathbf{n}_2$ ,  $\boldsymbol{\delta}_2 = -\mathbf{n}_1$ , and  $\boldsymbol{\delta}_3 = \mathbf{n}_1 - \mathbf{n}_2$ . In the Majorana fermion basis, these bands are associated with  $\zeta^3$  and  $\zeta^4$ , whereas the  $\zeta^1$  and  $\zeta^2$  fermions appear in the spectrum as zero-energy flat bands, see Fig. 5. The gap in the  $\zeta^{3,4}$  sector is of order  $|t'|$  if  $|t'| \ll |t|, |w|$ . We are mainly interested in the regime  $|t'| \sim |t| \sim |w| \gg |K|, |\lambda|$ , in which this gap is much larger than the interaction energy scale for the spin liquid. In this limit, we can project out the  $\zeta^{3,4}$  sector and the low-energy physics is governed by the coupling between the  $\zeta^{1,2}$  modes of the conduction electrons and the localized spins.

## B. Octupolar Kondo coupling

We now look for an on-site interaction that couples electrons to local moments and preserves time reversal symmetry. First, we note that the projection of the electron spin operator onto the sector of  $\zeta^{1,2}$  Majorana

fermions is given by

$$\begin{aligned} \mathcal{P}_{12} \Psi_j^\dagger \boldsymbol{\sigma} \Psi_j \mathcal{P}_{12} &= \frac{1}{2} \Psi_j^\dagger (\sigma^y - \rho^y) \Psi_j \hat{\mathbf{y}} \\ &= -i \zeta_j^1 \zeta_j^2 \hat{\mathbf{y}}, \end{aligned} \quad (22)$$

where  $\mathcal{P}_{12}$  is the projection operator. If the superconducting gap in the  $\zeta^{3,4}$  sector far exceeds all other energy scales, the operator in Eq. (22) is the only single-site electron operator active at low energies. We then consider the Kondo-like coupling

$$H_K = \frac{J_K}{2} \sum_j \Psi_j^\dagger (\sigma^y - \rho^y) \Psi_j T_j^{xyz}. \quad (23)$$

This interaction involves the octupole moment  $T_j^{xyz} \propto \tau_j^y$  of the localized spins. In terms of Majorana fermions, we have

$$H_K = J_K \sum_j \zeta_j^1 \zeta_j^2 \theta_j^x \theta_j^z. \quad (24)$$

To solve the Hamiltonian in Eq. (13), we note that we can pair the  $\theta_j^z$  Majorana fermion with either  $\zeta_j^1$  or  $\zeta_j^2$  to define the  $\mathbb{Z}_2$  operators

$$\hat{v}_j = -i \zeta_j^{\mu_j} \theta_j^z, \quad (25)$$

where  $\mu_j \in \{1, 2\}$  can be chosen independently at each site. It is straightforward to verify that these operators commute not only with one another, but also with the bond operators  $\hat{u}_{\langle ij \rangle}$  of the spin liquid and with the total Hamiltonian in Eq. (13). Thus,  $\hat{v}_j$  are conserved quantities and we can replace them by the eigenvalues  $\pm 1$  to obtain a quadratic Hamiltonian in the remaining Majorana fermions. Remarkably, a finite expectation value of the  $\hat{v}_j$  operators implies a hybridization between physical Majorana fermions defined from the conduction electrons and emergent Majorana fermions in the spin liquid. This type of hybridization has appeared in the literature as an order parameter for odd-frequency pairing in heavy-fermion superconductors [51, 52].

Since time reversal exchanges  $\zeta^1$  and  $\zeta^2$ , see Eq. (19), the choice of  $\mu_j = 1, 2$  for each  $\hat{v}_j$  breaks time reversal symmetry spontaneously. Thus, the Kondo coupling to the octupole moment of the spin liquid induces unconventional, time-reversal-symmetry-breaking superconductivity. To discuss the possible superconducting states, we must first assign values to the  $\mathbb{Z}_2$  variables. We consider two states that respect the translational symmetry of the honeycomb lattice: the uniform or “ferro” (F) configuration

$$\hat{v}_j^F = -i \zeta_j^1 \theta_j^z = 1 \quad \forall j, \quad (26)$$

and the staggered or “antiferro” (AF) configuration

$$\hat{v}_j^{\text{AF}} = \begin{cases} -i \zeta_j^1 \theta_j^z = 1, & \text{if } j \in \text{ sublattice A,} \\ -i \zeta_j^2 \theta_j^z = 1, & \text{if } j \in \text{ sublattice B.} \end{cases} \quad (27)$$

Changing the sign of  $\hat{v}_j$  does not affect any physical observables, due to the gauge symmetry  $(\eta_j^\alpha, \theta_j^\alpha) \mapsto (-\eta_j^\alpha, -\theta_j^\alpha)$  of the Majorana fermion representation in the spin liquid sector. The Kondo coupling for F and AF configurations becomes, respectively,

$$H_K^F = i J_K \sum_j \zeta_j^2 \theta_j^x, \quad (28)$$

$$H_K^{\text{AF}} = i J_K \sum_{j \in \text{A}} \zeta_j^2 \theta_j^x - i J_K \sum_{j \in \text{B}} \zeta_j^1 \theta_j^x. \quad (29)$$

In order to obtain the energy spectrum with finite Kondo interaction, we define the spinors

$$\Upsilon_F(\mathbf{k}) = \begin{pmatrix} \theta_A^x(\mathbf{k}) \\ \theta_B^x(\mathbf{k}) \\ \theta_A^y(\mathbf{k}) \\ \theta_B^y(\mathbf{k}) \\ \zeta_A^2(\mathbf{k}) \\ \zeta_B^2(\mathbf{k}) \end{pmatrix}, \quad \Upsilon_{\text{AF}}(\mathbf{k}) = \begin{pmatrix} \theta_A^x(\mathbf{k}) \\ \theta_B^x(\mathbf{k}) \\ \theta_A^y(\mathbf{k}) \\ \theta_B^y(\mathbf{k}) \\ \zeta_A^2(\mathbf{k}) \\ -\zeta_B^1(\mathbf{k}) \end{pmatrix}, \quad (30)$$

which contain the Majorana fermions that acquire a dispersion at low energies. The total Hamiltonian has the form

$$\mathcal{P}_{12} H^{F/\text{AF}} \mathcal{P}_{12} = \sum_{\mathbf{k}} \Upsilon_{F/\text{AF}}^\dagger(\mathbf{k}) \mathcal{H}(\mathbf{k}) \Upsilon_{F/\text{AF}}(\mathbf{k}), \quad (31)$$

where the antisymmetric matrix  $\mathcal{H}(\mathbf{k})$  is the same for both uniform and staggered configurations:

$$\mathcal{H}(\mathbf{k}) = \begin{pmatrix} \mathcal{H}_s(\mathbf{k}) & V^\dagger \\ V & \mathbb{0}_2 \end{pmatrix}, \quad (32)$$

with  $\mathbb{0}_2$  the  $2 \times 2$  null matrix,

$$\mathcal{H}_s(\mathbf{k}) = \begin{pmatrix} 0 & 0 & i\lambda & 0 \\ 0 & 0 & 0 & i\lambda \\ -i\lambda & 0 & 0 & ig(\mathbf{k}) \\ 0 & -i\lambda & -ig^*(\mathbf{k}) & 0 \end{pmatrix}, \quad (33)$$

and

$$V = \begin{pmatrix} -iJ_K & 0 & 0 & 0 \\ 0 & -iJ_K & 0 & 0 \end{pmatrix}. \quad (34)$$

Thus, F and AF states share the same energy spectrum illustrated in Fig. 6. We see that the Majorana fermions that appear in the Kondo coupling Eqs. (28) and (29) give rise to a gapless band structure with a Dirac node at the K point. This represents the dispersion of the Bogoliubov quasiparticles in this nodal superconductor. There are no zero-energy flat bands left. The dispersion relations for the decoupled  $\zeta^{3,4}$  modes are given by Eq. (21) and appear at much higher energies provided that  $|t| \sim |t'| \sim |w| \gg |K|, |\lambda|, |J_K|$ .

Since we obtain the same spectrum for F and AF configurations, these two states have exactly the same

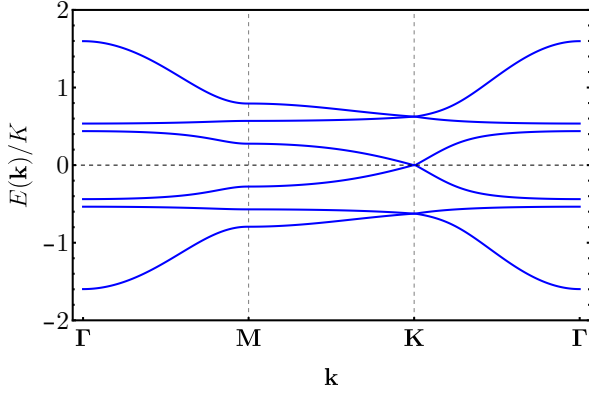


FIG. 6. Dispersion relation of Majorana fermions in both F and AF configurations of the coupled system. Here we set  $\lambda/K = 0.75$  and  $J_K/K = 1$ . The bands associated with the decoupled  $\zeta^3$  and  $\zeta^4$  Majorana fermions appear at much higher energies and are not shown.

ground state energy. This degeneracy can be traced back to a local  $SO(2)$  symmetry of the exactly solvable model. We can regard  $\zeta_j^1$  and  $\zeta_j^2$  as the real and imaginary parts of a complex fermion defined at each site. The choice of real and imaginary parts can be parametrized by a rotation in the complex plane, i.e., the phase of the complex fermion. This choice is arbitrary and can be made locally at each site because these Majorana modes only appear in the Kondo coupling Eq. (24). As we shall discuss in Sec. V, the degeneracy between F and AF states is lifted once we add integrability-breaking perturbations that couple  $\zeta^1$  and  $\zeta^2$  at different sites and remove the local  $SO(2)$  symmetry.

Interestingly, despite the spontaneous time reversal symmetry breaking, the local magnetization vanishes exactly in the ground state of the exactly solvable model:

$$\langle \Psi_j^\dagger \sigma \Psi_j \rangle = 0, \quad \langle \mathbf{J}_j \rangle = 0. \quad (35)$$

The reason is that both the electron and local moment spin operators contain Majorana fermions absorbed into the  $\mathbb{Z}_2$  operators, whose action on a given eigenstate changes the sector of  $\mathbb{Z}_2$  fluxes. Local time-reversal-odd operators that acquire a nonzero expectation value must involve a product of electron and local-moment operators, for instance,

$$\begin{aligned} \langle O_j^{x^2-y^2} \Psi_j^\dagger \sigma^y \Psi_j \rangle &\sim \langle \theta_j^y \theta_j^z \zeta_j^1 \zeta_j^2 \rangle \\ &\sim \langle \zeta_j^1 \theta_j^z \rangle \langle \zeta_j^2 \theta_j^y \rangle \neq 0, \end{aligned} \quad (36)$$

where the factor  $\langle \zeta_j^2 \theta_j^y \rangle$  is nonzero because  $\lambda \neq 0$  mixes  $\theta_j^y$  with  $\theta_j^x$  and the operator  $\zeta_j^2 \theta_j^x$  appears in the Kondo coupling in Eq. (28). This provides an example of a composite order parameter [59–63] or vestigial order [64].

#### IV. EFFECTIVE ACTION FOR ELECTRONS IN THE COUPLED SYSTEM

In this section, we investigate the effect of the octupolar Kondo coupling on the superconducting properties of the coupled system. Since the Hamiltonian becomes quadratic after fixing the values of the  $\mathbb{Z}_2$  variables, we can integrate out the Majorana fermions of the quadrupolar spin liquid to derive an exact effective action for the conduction electrons. We are mainly interested in the pairing amplitudes generated by the Kondo coupling which manifest the breaking of time reversal symmetry. We find that, while the uniform and staggered configurations are degenerate within the exactly solvable model, they produce different superconducting order parameters because the physical Majorana fermions  $\zeta^1$  and  $\zeta^2$  are associated with different electronic spin states, see Eq. (18). More details of the calculations are given in Appendix B.

##### A. Superconducting state in the F configuration

For the uniform state with the Kondo interaction  $H_K^F$  in Eq. (28), the effective action obtained after integrating out the Majorana fermions  $\theta^x$  and  $\theta^y$  has the form

$$\mathcal{S}_F = \sum_{\mathbf{k}, \omega_n} \Psi^\dagger(\mathbf{k}, i\omega_n) [i\omega_n - \mathcal{H}_c(\mathbf{k}) - \Sigma_F(\mathbf{k}, i\omega_n)] \Psi(\mathbf{k}, i\omega_n), \quad (37)$$

where  $\omega_n$  are Matsubara frequencies and  $\Psi(\mathbf{k}, i\omega_n)$  is the Balian-Werthamer spinor in momentum-frequency space:

$$\Psi(\mathbf{k}, i\omega_n) = \begin{pmatrix} \Psi_A(\mathbf{k}, i\omega_n) \\ \Psi_B(\mathbf{k}, i\omega_n) \end{pmatrix}, \quad (38)$$

with

$$\Psi_{A/B}(\mathbf{k}, i\omega_n) = \begin{pmatrix} \psi_{A/B}(\mathbf{k}, i\omega_n) \\ -i\sigma^y [\psi_{A/B}^\dagger(-\mathbf{k}, -i\omega_n)]^T \end{pmatrix}. \quad (39)$$

Here  $\mathcal{H}_c(\mathbf{k})$  is the matrix obtained by Fourier transforming  $H_c$  in Eq. (14), see Appendix B. The self-energy  $\Sigma_F(\mathbf{k}, i\omega_n)$  is due to the hybridization of the conduction electrons with the Majorana fermions of the spin liquid and is of order  $J_K^2$ .

The effective action in Eq. (37) contains three terms: a normal (N), a superconducting (SC), and a resonant-exchange (RE) part. The N and RE parts are written explicitly in Appendix B. Here we discuss only the contribution from the Kondo coupling to the SC part, which has the form

$$\begin{aligned} \delta \mathcal{S}_F^{\text{SC}} = \sum_{\mathbf{k}, \omega_n} \sum_{b, b'} & [\psi_b^T(-\mathbf{k}, -i\omega_n) \sigma^y \Delta_{bb'}^{\text{SC}}(\mathbf{k}, i\omega_n) \psi_{b'}(\mathbf{k}, i\omega_n) \\ & + \text{H.c.}], \end{aligned} \quad (40)$$



where  $b, b'$  are sublattice indices. The induced pairing functions are given by

$$\begin{aligned}\Delta_{AA}^{\text{SC}}(\mathbf{k}, i\omega_n) &= \frac{J_K^2}{2} \frac{\omega_n(\omega_n^2 + |g(\mathbf{k})|^2 + \lambda^2)\sigma^+}{(\omega_n^2 + \lambda^2)^2 + |g(\mathbf{k})|^2\omega_n^2}, \\ \Delta_{AB}^{\text{SC}}(\mathbf{k}, i\omega_n) &= -\frac{J_K^2}{2} \frac{\lambda^2 g(\mathbf{k})\sigma^+}{(\omega_n^2 + \lambda^2)^2 + |g(\mathbf{k})|^2\omega_n^2}, \\ \Delta_{BA}^{\text{SC}}(\mathbf{k}, i\omega_n) &= \frac{J_K^2}{2} \frac{\lambda^2 g^*(\mathbf{k})\sigma^+}{(\omega_n^2 + \lambda^2)^2 + |g(\mathbf{k})|^2\omega_n^2}, \\ \Delta_{BB}^{\text{SC}}(\mathbf{k}, i\omega_n) &= \frac{J_K^2}{2} \frac{\omega_n(\omega_n^2 + |g(\mathbf{k})|^2 + \lambda^2)\sigma^+}{(\omega_n^2 + \lambda^2)^2 + |g(\mathbf{k})|^2\omega_n^2},\end{aligned}\quad (41)$$

where  $\sigma^\pm = (\sigma^x \pm i\sigma^y)/2$ . Therefore, the Kondo coupling gives rise to triplet pairing with both even- and odd-frequency amplitudes. Exactly at the K point, where  $g(\mathbf{k})$  vanishes for  $K_\gamma = K$ , the AB and BA components vanish, whereas the AA and BB components scale linearly with frequency,  $\Delta_{bb}^{\text{SC}} \sim (J_K/\lambda)^2 \omega_n \sigma^\pm$  for  $|\omega_n| \ll |\lambda|$ . This result bears a close resemblance to mean-field theories for related Kondo lattice models [52, 53, 65].

### B. Superconducting state in the AF configuration

We repeat the procedure of Sec. IV A for the staggered state with the Kondo interaction given in Eq. (29). The effective action in this case also exhibits N, SC and RE contributions. The superconducting part generated by the Kondo coupling in the AF case reads

$$\delta\mathcal{S}_{\text{AF}}^{\text{SC}} = \sum_{\mathbf{k}, \omega_n} \sum_{b, b'} [\psi_b^T(-\mathbf{k}, -i\omega_n) \sigma^y \tilde{\Delta}_{bb'}^{\text{SC}}(\mathbf{k}, i\omega_n) \psi_{b'}(\mathbf{k}, i\omega_n) + \text{H.c.}], \quad (42)$$

where

$$\begin{aligned}\tilde{\Delta}_{AA}^{\text{SC}}(\mathbf{k}, i\omega_n) &= \frac{J_K^2}{2} \frac{\omega_n(\omega_n^2 + |g(\mathbf{k})|^2 + \lambda^2)\sigma^+}{(\omega_n^2 + \lambda^2)^2 + |g(\mathbf{k})|^2\omega_n^2}, \\ \tilde{\Delta}_{AB}^{\text{SC}}(\mathbf{k}, i\omega_n) &= \frac{J_K^2}{4} \frac{\lambda^2 g(\mathbf{k})(\mathbb{1}_2 + \sigma^z)}{(\omega_n^2 + \lambda^2)^2 + |g(\mathbf{k})|^2\omega_n^2}, \\ \tilde{\Delta}_{BA}^{\text{SC}}(\mathbf{k}, i\omega_n) &= \frac{J_K^2}{4} \frac{\lambda^2 g^*(\mathbf{k})(\mathbb{1}_2 - \sigma^z)}{(\omega_n^2 + \lambda^2)^2 + |g(\mathbf{k})|^2\omega_n^2}, \\ \tilde{\Delta}_{BB}^{\text{SC}}(\mathbf{k}, i\omega_n) &= -\frac{J_K^2}{2} \frac{\omega_n(\omega_n^2 + |g(\mathbf{k})|^2 + \lambda^2)\sigma^-}{(\omega_n^2 + \lambda^2)^2 + |g(\mathbf{k})|^2\omega_n^2}.\end{aligned}\quad (43)$$

These pairing functions also involve a mixture of even- and odd-frequency pairing. However, they are markedly different from those in the uniform configuration, since now the AB and BA components exhibit a superposition of singlet and triplet pairings. Moreover, the AA and BB components differ in the spin dependence of the triplet pairing. At the K point,  $\Delta_{AA}^{\text{SC}} \sim (J_K/\lambda)^2 \omega_n \sigma^+$  for the A sublattice, but  $\Delta_{BB}^{\text{SC}} \sim (J_K/\lambda)^2 \omega_n \sigma^-$  for the B sublattice.

## V. INTEGRABILITY-BREAKING PERTURBATIONS

In this section, we go beyond the exactly solvable model to examine whether perturbations may lift the degeneracy between the F and AF configurations. Rather than discuss all symmetry-allowed perturbations, we focus on the effects of additional quadratic terms in the conduction electron Hamiltonian that involve the Majorana fermions  $\zeta^1$  and  $\zeta^2$ . We consider

$$\begin{aligned}\delta H_c &= i \sum_{\langle jl \rangle} [\delta t_{jl}(\zeta_j^1 \zeta_l^2 + \zeta_j^2 \zeta_l^1) + \delta w_{jl}(\zeta_j^1 \zeta_l^1 - \zeta_j^2 \zeta_l^2)] \\ &\quad + i \sum_{\langle\langle jl \rangle\rangle} [\delta t'_{jl}(\zeta_j^1 \zeta_l^2 + \zeta_j^2 \zeta_l^1) + \delta w'_{jl}(\zeta_j^1 \zeta_l^1 - \zeta_j^2 \zeta_l^2)],\end{aligned}\quad (44)$$

where we fix the values of  $\delta t_{jl} = \pm \delta t$ ,  $\delta w_{jl} = \pm \delta w$ ,  $\delta t'_{jl} = \pm \delta t'$  and  $\delta w'_{jl} = \pm \delta w'$  according to the orientation of the nearest and next-nearest-neighbor links as explained in Sec. III A. In terms of the Balian-Werthamer spinor [see Eq. (15)],  $\delta H_c$  assumes the form

$$\delta H_c = \sum_{\langle jl \rangle} \Psi_j^\dagger M_{jl} \Psi_l + \sum_{\langle\langle jl \rangle\rangle} \Psi_j^\dagger M'_{jl} \Psi_l, \quad (45)$$

with

$$\begin{aligned}M_{jl} &= i\delta t_{jl}(\sigma^x \rho^z - \sigma^z \rho^x) + i\delta w_{jl}(\sigma^z \rho^z + \sigma^x \rho^x), \\ M'_{jl} &= i\delta t'_{jl}(\sigma^x \rho^z - \sigma^z \rho^x) + i\delta w'_{jl}(\sigma^z \rho^z + \sigma^x \rho^x).\end{aligned}\quad (46)$$

Since the  $\mathbb{Z}_2$  operators  $\hat{v}_j$  defined in Eq. (25) do not commute with  $\delta H_c$ , this perturbation breaks the integrability of the model. Here we shall assume that  $|\delta t|, |\delta w|, |\delta t'|, |\delta w'| \ll |K|, |\lambda|, |J_K|$  so that the  $\mathbb{Z}_2$  variables are still good order parameters with expectation value  $\langle \hat{v}_j \rangle \approx 1$ . One consequence of the perturbation is that the Majorana fermions absorbed into  $\hat{v}_j$  must acquire a small dispersion. Nevertheless, as long as the latter remain gapped, this should not affect qualitative properties of the low-energy spectrum discussed in the following.

In the spirit of first-order perturbation theory, we project  $\delta H_c$  onto the low-energy subspace where the Majorana fermions contained in  $\hat{v}_j$  are gapped out and cannot be excited. For the F configuration, this rules out the terms involving  $\zeta^1$  altogether. As a result, we obtain the projected perturbation

$$\delta H_c^{\text{F}} = -i \sum_{\langle jl \rangle} \delta w_{jl} \zeta_j^2 \zeta_l^2 - i \sum_{\langle\langle jl \rangle\rangle} \delta w'_{jl} \zeta_j^2 \zeta_l^2. \quad (47)$$

In contrast, in the AF configuration the fermionic excitations related to  $\zeta^1$  become gapped only in sublattice A, while those related to  $\zeta^2$  are gapped in sublattice B. Con-

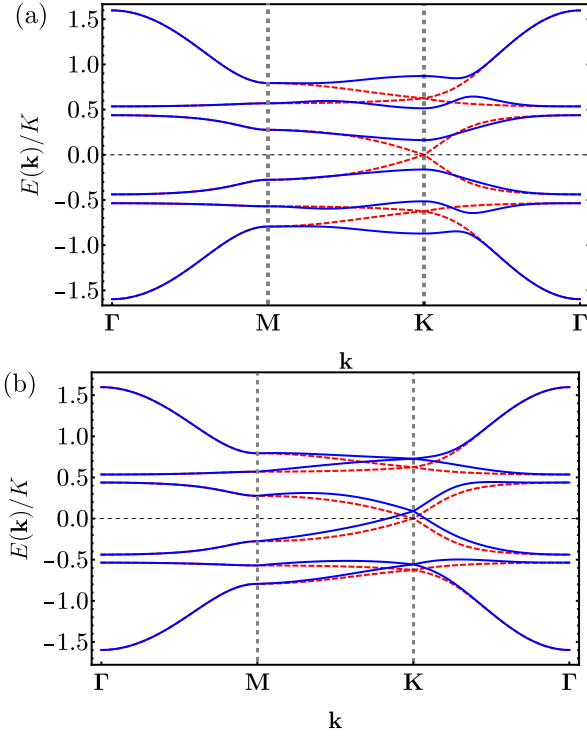


FIG. 7. Low-energy bands of the coupled system including the integrability-breaking perturbations in the (a) F configuration and (b) AF configuration. Here we use  $\lambda/K = 0.75$ ,  $J_K/K = 1$  and  $\delta t = \delta w = 0$ . The solid lines show the result for  $\delta w'/K = 0.2$ , which can be compared with the dispersion for the exactly solvable model ( $\delta w' = 0$ ) given by the dashed lines. For the F state, a small  $\delta w'$  opens a gap at the K point. For the AF state, it induces the formation of a Bogoliubov Fermi surface.

sequently, the projection of  $\delta H_c$  for the AF state yields

$$\begin{aligned} \delta H_c^{\text{AF}} = & i \sum_{\substack{\langle j l \rangle \\ j \in B}} \delta t_{jl} \zeta_j^1 \zeta_l^2 + i \sum_{\substack{\langle \langle j l \rangle \rangle \\ j \in B}} \delta w'_{jl} \zeta_j^1 \zeta_l^1 \\ & - i \sum_{\substack{\langle \langle j l \rangle \rangle \\ j \in A}} \delta w'_{jl} \zeta_j^2 \zeta_l^2. \end{aligned} \quad (48)$$

Note that both  $\delta H_c^{\text{F}}$  and  $\delta H_c^{\text{AF}}$  remove the local  $\text{SO}(2)$  symmetry that exchanges  $\zeta_j^1$  and  $\zeta_j^2$ , see Sec. III B.

We add the terms in Eqs. (47) and (48) to the Hamiltonian for the coupled system in the F and AF configurations, respectively, and recalculate the spectrum by taking the Fourier transform of the Majorana fermion operators. The dispersion relations are shown in Fig. 7. We find that the degeneracy between F and AF states is lifted by a finite next-nearest-neighbor coupling  $\delta w'$ . The latter produces a gap in the excitation spectrum for the F state, while for the AF state it turns the Dirac point into a Bogoliubov Fermi surface [54]. The ground state energies of the two configurations are now clearly different, and either state can have lower energy depending on the values of  $\delta t$ ,  $\delta w$  and  $\delta w'$ .

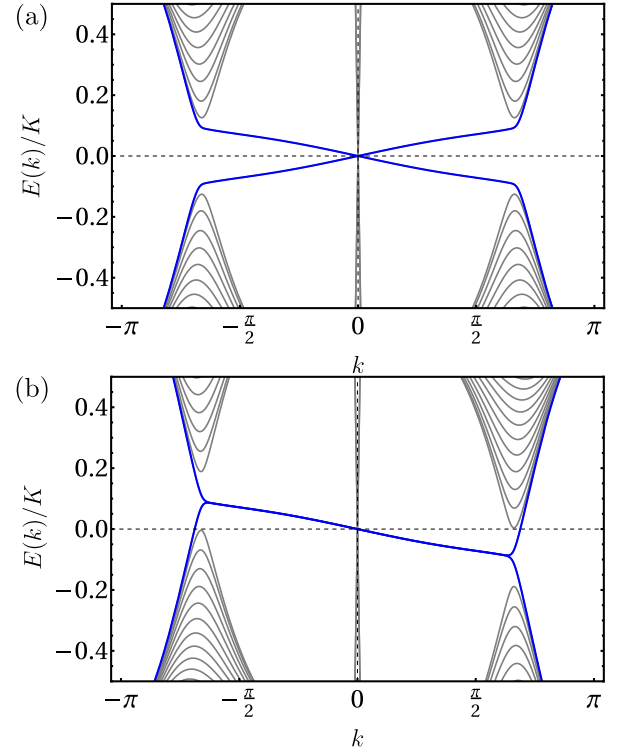


FIG. 8. Band structure of the perturbed model for the coupled system with open boundary conditions in the  $y$  direction and width  $W = 60$  unit cells. Here we set  $J_K/K = 1$ ,  $\lambda/K = 0.75$ , and  $\delta t/K = \delta w/K = \delta w'/K = 0.1$ . Panel (a) shows the spectrum for the F state. The blue lines highlight the gapless edge states associated with the low-energy Majorana fermions. We also show the pair of edge states associated with the  $\zeta^{3,4}$  sector of the conduction electrons, whose bulk excitations appear at much higher energies. The parameters in this sector are set to  $t/K = w/K = 10$  and  $t'/K = 5$ . Panel (b) shows the spectrum for the AF state. In this case we find antichiral edge states.

We also investigated the presence of edge states for the perturbed superconducting states on a strip geometry. The results are presented in Fig. 8. For both F and AF states, there exist pairs of gapless edge mode due to the nontrivial topological nature of the phase. The perturbed F state is a gapped superconductor with counter-propagating chiral edge modes localized at opposite edges of the strip. On the other hand, the AF state has edge states that propagate in the same direction, and whose equilibrium current is compensated by that of the gapless bulk modes. This is a superconducting version of the antichiral edge states discussed in Ref. [55]. Note that both types of band structures shown in Fig. 8 are only possible once time reversal symmetry is broken.

## VI. CONCLUSIONS

We proposed an exactly solvable model for interacting  $j_{\text{eff}} = \frac{3}{2}$  local moments on the honeycomb lattice. Our

proposal is guided by symmetry properties and by a Majorana fermion representation of the multipole operators. We first analyzed a time-reversal-invariant spin model that includes bond-dependent quadrupole-quadrupole interactions and a single-ion anisotropy term. To obtain a solvable spin Hamiltonian with no zero-energy flat bands, we added terms that break time reversal symmetry explicitly and found a gapped chiral spin liquid.

We also investigated the coupling of the time-reversal-invariant quadrupolar spin liquid to a superconductor, with the goal of constructing an exactly solvable model in which the Majorana fermions in the spin liquid hybridize with itinerant electrons. The conserved  $\mathbb{Z}_2$  variables defined in the octupolar Kondo coupling are related to the order parameter for odd-frequency pairing in heavy-fermion superconductors [51, 52]. Indeed, we find that this Kondo coupling breaks time reversal symmetry spontaneously and generates odd-frequency pairing in the effective action for the conduction electrons. The result within the exactly solvable model is a gapless time-reversal-symmetry-breaking superconductor. Perturbing the model with integrability breaking terms, we obtained either a gapped chiral superconductor or a Bogoliubov Fermi surface state, both of which exhibit topologically protected (chiral or antichiral) edge states.

Our results illustrate the possibility of inducing new topological phases by coupling two subsystems which may or may not have topological properties by themselves. This observation is in line with the bulk topological proximity effect introduced in Refs. [66, 67] and with the proposal of topological superconductivity in the Kondo-Kitaev model [45]. Also noteworthy is the recent experimental evidence for odd-frequency superconductivity at the interface between a topological insulator and a conventional superconductor [68]. The models studied here may be particularly relevant to rare-earth materials with strong quadrupole-quadrupole interactions between localized spins, which may also be coupled to itinerant electrons. Moreover, the spin-orbital physics that we discussed in the context of  $j_{\text{eff}} = \frac{3}{2}$  systems could be applied to correlated Moiré systems [69, 70] and heterostructures [71] with orbital/valley degrees of freedom.

## ACKNOWLEDGMENTS

We thank M. M. de Oliveira, V. Quito, and S. Trebst for stimulating discussions. We are grateful to F. Ramos for checking the ground state energy and degeneracy of the spin model with exact diagonalization. Financial support from CPNq is acknowledged by C.S.deF. (project No. 435665/2016-2), E.M. (307041/2017-4) and R.G.P. (303298/2019-7). E.M. and R.G.P. also acknowledge Capes/Cofecub 0899/2018. V.S.deC. thanks the financial support from FAPESP and CAPES under Grants Nos. 2016/05069-7 and 88887.469170/2019-00, respectively. Research at IIP-UFRN is supported by Brazilian ministries MEC and MCTIC.

### Appendix A: Majorana fermion representation

In this appendix, we discuss the transformation of the Majorana fermions in the spin liquid under time reversal.

At each site, we can combine the six Majorana fermions  $(\eta^\alpha, \theta^\alpha)$  to define three complex fermions:

$$\begin{aligned} c^x &= \frac{1}{2}(\eta^x - i\theta^x), \\ c^y &= \frac{1}{2}(\eta^y - i\theta^y), \\ c^z &= \frac{1}{2}(\eta^z - i\theta^z), \end{aligned} \quad (\text{A1})$$

which obey  $\{c^\alpha, (c^\beta)^\dagger\} = \delta^{\alpha\beta}$ . States in this Fock space are specified by  $|n_x, n_y, n_z\rangle$ , where  $n_\alpha \in \{0, 1\}$  are the fermion occupation numbers. Thus, this representation generates 8 states, which is twice the size of the physical Hilbert space for spin 3/2. We can represent the four eigenstates of  $J^z$  by identifying

$$\begin{aligned} \left|\frac{3}{2}\right\rangle &= |0, 0, 0\rangle \equiv |\emptyset\rangle, \\ \left|\frac{1}{2}\right\rangle &= |1, 1, 0\rangle = (c^x)^\dagger (c^y)^\dagger |\emptyset\rangle, \\ \left|-\frac{1}{2}\right\rangle &= |0, 1, 1\rangle = (c^y)^\dagger (c^z)^\dagger |\emptyset\rangle, \\ \left|-\frac{3}{2}\right\rangle &= |1, 0, 1\rangle = (c^x)^\dagger (c^z)^\dagger |\emptyset\rangle. \end{aligned} \quad (\text{A2})$$

This corresponds to imposing the parity constraint

$$(2n_x - 1)(2n_y - 1)(2n_z - 1) = -1, \quad (\text{A3})$$

which in terms of Majorana fermions becomes Eq. (6).

Since time reversal acts on the spin-3/2 states as

$$\begin{aligned} T\left|\frac{3}{2}\right\rangle &= \left|-\frac{3}{2}\right\rangle, & T\left|\frac{1}{2}\right\rangle &= -\left|-\frac{1}{2}\right\rangle, \\ T\left|-\frac{1}{2}\right\rangle &= \left|\frac{1}{2}\right\rangle, & T\left|-\frac{3}{2}\right\rangle &= -\left|\frac{3}{2}\right\rangle, \end{aligned} \quad (\text{A4})$$

we postulate that time reversal is equivalent to a particle-hole transformation for fermions  $c^x$  and  $c^z$ , such that  $Tc^{x,z}T^{-1} = (c^{x,z})^\dagger$  and  $T|0, 0, 0\rangle = |1, 0, 1\rangle$ . We can then check that

$$\begin{aligned} T\left|-\frac{3}{2}\right\rangle &= T(c^x)^\dagger (c^z)^\dagger |\emptyset\rangle \\ &= c^x c^z T|\emptyset\rangle \\ &= c^x c^z (c^x)^\dagger (c^z)^\dagger |\emptyset\rangle \\ &= -|\emptyset\rangle, \end{aligned} \quad (\text{A5})$$

as expected. Likewise, it is straightforward to verify the time reversal transformation of the  $|\pm\frac{1}{2}\rangle$  states. The rule of particle-hole transformation for  $c^x$  and  $c^z$  but not for  $c^y$  is equivalent to applying complex conjugation and taking  $\theta^y \mapsto -\theta^y$ , as mentioned in Sec. II B.

## Appendix B: Effective action

In this appendix, we provide details about the calculation of the effective action discussed in Sec. IV. The term  $\mathcal{H}_c(\mathbf{k})$  in Eq. (37) is the Hamiltonian matrix obtained by Fourier transforming  $H_c$  in Eq. (14), which written as matrix in sublattice space becomes

$$\mathcal{H}_c(\mathbf{k}) = \frac{1}{2} \begin{pmatrix} \Delta_0(\mathbf{k})(\sigma^x \rho^z + \sigma^z \rho^x) & if(\mathbf{k})[t(\sigma^x \rho^z + \sigma^z \rho^x) + w(\sigma^z \rho^z - \sigma^x \rho^x)] \\ -if^*(\mathbf{k})[t(\sigma^x \rho^z + \sigma^z \rho^x) + w(\sigma^z \rho^z - \sigma^x \rho^x)] & -\Delta_0(\mathbf{k})(\sigma^x \rho^z + \sigma^z \rho^x) \end{pmatrix}. \quad (\text{B1})$$

In this form, it is easy to see that  $\mathcal{H}_c(\mathbf{k})$  already contains triplet pairing correlations. However, we want to address the contributions contained in the electron self-energy, which has the form

$$\Sigma_{\text{F/AF}}(\mathbf{k}, i\omega_n) = \mathcal{V}_{\text{F/AF}} \frac{1}{i\omega_n - \mathcal{H}_s(\mathbf{k})} \mathcal{V}_{\text{F/AF}}^\dagger, \quad (\text{B2})$$

where  $\mathcal{H}_s(\mathbf{k})$  is given in Eq. (33) and  $\mathcal{V}_{\text{F/AF}}$  are hybridization matrices between the Balian-Werthamer spinor and the Majorana fermions in the spin liquid.

### 1. Uniform configuration

For the F state, the hybridization matrix is

$$\mathcal{V}_{\text{F}}^\dagger = \frac{iJ_K}{\sqrt{2}} \begin{pmatrix} 0 & 0 & 0 & 0 & 0 & 0 & 0 & 0 \\ 0 & 0 & 0 & 0 & 0 & 0 & 0 & 0 \\ 0 & -1 & 1 & 0 & 0 & 0 & 0 & 0 \\ 0 & 0 & 0 & 0 & 0 & -1 & 1 & 0 \end{pmatrix}. \quad (\text{B3})$$

Substituting the above expression into Eq. (B2), we obtain the self-energy

$$\Sigma_{\text{F}}(\mathbf{k}, i\omega_n) = \frac{J_K^2}{2} (\mathbb{1}_4 - \boldsymbol{\sigma} \cdot \boldsymbol{\rho}) \otimes \mathcal{M}(\mathbf{k}, i\omega_n), \quad (\text{B4})$$

where we introduce the matrix in sublattice space

$$\mathcal{M}(\mathbf{k}, i\omega_n) = \begin{pmatrix} i\Omega(\mathbf{k}, i\omega_n) & i\Gamma(\mathbf{k}, i\omega_n) \\ -i\Gamma^*(\mathbf{k}, i\omega_n) & i\Omega(\mathbf{k}, i\omega_n) \end{pmatrix}, \quad (\text{B5})$$

with the following functions:

$$\Omega(\mathbf{k}, i\omega_n) = -\frac{\omega_n[\omega_n^2 + |g(\mathbf{k})|^2 + \lambda^2]}{2[(\omega_n^2 + \lambda^2)^2 + |g(\mathbf{k})|^2\omega_n^2]}, \quad (\text{B6})$$

$$\Gamma(\mathbf{k}, i\omega_n) = \frac{\lambda^2 g(\mathbf{k})}{2[(\omega_n^2 + \lambda^2)^2 + |g(\mathbf{k})|^2\omega_n^2]}. \quad (\text{B7})$$

As done in Ref. [52], we decompose  $\Sigma_{\text{F}}(\mathbf{k}, i\omega_n)$  into three terms:

$$\Sigma_{\text{F}}(\mathbf{k}, i\omega_n) = \Sigma_{\text{F}}^{\text{N}}(\mathbf{k}, i\omega_n) + \Sigma_{\text{F}}^{\text{SC}}(\mathbf{k}, i\omega_n) + \Sigma_{\text{F}}^{\text{RE}}(\mathbf{k}, i\omega_n), \quad (\text{B8})$$

where

$$\begin{aligned} \Sigma_{\text{F}}^{\text{N}}(\mathbf{k}, i\omega_n) &= \frac{J_K^2}{2} \mathbb{1}_4 \otimes \mathcal{M}(\mathbf{k}, i\omega_n), \\ \Sigma_{\text{F}}^{\text{SC}}(\mathbf{k}, i\omega_n) &= -\frac{J_K^2}{4} (\sigma^+ \rho^- + \sigma^- \rho^+) \otimes \mathcal{M}(\mathbf{k}, i\omega_n), \\ \Sigma_{\text{F}}^{\text{RE}}(\mathbf{k}, i\omega_n) &= -\frac{J_K^2}{2} \sigma^z \rho^z \otimes \mathcal{M}(\mathbf{k}, i\omega_n). \end{aligned} \quad (\text{B9})$$

Expressing the action in terms of the two-component spinors  $\psi_{A/B}(\mathbf{k}, i\omega_n)$ , we find the superconducting action and pairing function written in Eqs. (40) and (41), respectively.

Proceeding rather similarly, the induced RE action in the F state is obtained as

$$\delta\mathcal{S}_{\text{RE}} = \sum_{\mathbf{k}, \omega_n} \sum_{b, b'} [\psi_b^\dagger(\mathbf{k}, i\omega_n) \chi_{bb'}^{\text{RE}}(\mathbf{k}, i\omega_n) \psi_{b'}(\mathbf{k}, i\omega_n) + \text{H.c.}], \quad (\text{B10})$$

where

$$\begin{aligned} \chi_{\text{AA}}^{\text{RE}}(\mathbf{k}, i\omega_n) &= -\frac{iJ_K^2}{4} \frac{\omega_n(\omega_n^2 + |g(\mathbf{k})|^2 + \lambda^2)\sigma^z}{(\omega_n^2 + \lambda^2)^2 + |g(\mathbf{k})|^2\omega_n^2}, \\ \chi_{\text{AB}}^{\text{RE}}(\mathbf{k}, i\omega_n) &= \frac{iJ_K^2}{4} \frac{\lambda^2 g(\mathbf{k})\sigma^z}{(\omega_n^2 + \lambda^2)^2 + |g(\mathbf{k})|^2\omega_n^2}, \\ \chi_{\text{BA}}^{\text{RE}}(\mathbf{k}, i\omega_n) &= -\frac{iJ_K^2}{4} \frac{\lambda^2 g^*(\mathbf{k})\sigma^z}{(\omega_n^2 + \lambda^2)^2 + |g(\mathbf{k})|^2\omega_n^2}, \\ \chi_{\text{BB}}^{\text{RE}}(\mathbf{k}, i\omega_n) &= -\frac{iJ_K^2}{4} \frac{\omega_n(\omega_n^2 + |g(\mathbf{k})|^2 + \lambda^2)\sigma^z}{(\omega_n^2 + \lambda^2)^2 + |g(\mathbf{k})|^2\omega_n^2}. \end{aligned} \quad (\text{B11})$$

The above order parameters indicate the emergence of a nonlocal order, which is completely polarized along the  $z$  direction.

### 2. Staggered configuration

The procedure to calculate the induced SC and RE actions for the AF state follows the same steps described in the last subsection. The hybridization matrix in this case is

$$\mathcal{V}_{\text{AF}}^\dagger = \frac{iJ_K}{\sqrt{2}} \begin{pmatrix} 0 & 0 & 0 & 0 & 0 & 0 & 0 & 0 \\ 0 & 0 & 0 & 0 & 0 & 0 & 0 & 0 \\ 0 & -1 & 1 & 0 & 0 & 0 & 0 & 0 \\ 0 & 0 & 0 & 0 & 1 & 0 & 0 & 1 \end{pmatrix}. \quad (\text{B12})$$

The self-energy in Eq. (B2) has the form

$$\Sigma_{\text{AF}}(\mathbf{k}, i\omega_n) = \Sigma_{\text{AF}}^{\text{N}}(\mathbf{k}, i\omega_n) + \Sigma_{\text{AF}}^{\text{SC}}(\mathbf{k}, i\omega_n) + \Sigma_{\text{AF}}^{\text{RE}}(\mathbf{k}, i\omega_n), \quad (\text{B13})$$

where

$$\begin{aligned}
\Sigma_{\text{AF}}^{\text{N}}(\mathbf{k}, i\omega_n) &= \frac{J_K^2}{2} \mathbb{1}_4 \otimes i\Omega(\mathbf{k}, i\omega_n) \\
\Sigma_{\text{AF}}^{\text{SC}}(\mathbf{k}, i\omega_n) &= \frac{J_K^2}{2} \begin{pmatrix} -i\Omega(\mathbf{k}, i\omega_n)(\rho^x \sigma^x + \rho^y \sigma^y) & \Gamma(\mathbf{k}, i\omega_n)(\rho^y + i\rho^x \sigma^z) \\ \Gamma^*(\mathbf{k}, i\omega_n)(\rho^y - i\rho^x \sigma^z) & i\Omega(\mathbf{k}, i\omega_n)(\rho^x \sigma^x + \rho^y \sigma^y) \end{pmatrix}, \\
\Sigma_{\text{AF}}^{\text{RE}}(\mathbf{k}, i\omega_n) &= \frac{J_K^2}{2} \begin{pmatrix} -i\Omega(\mathbf{k}, i\omega_n)\rho^z \sigma^z & -\Gamma(\mathbf{k}, i\omega_n)(\sigma^y + i\rho^z \sigma^x) \\ -\Gamma^*(\mathbf{k}, i\omega_n)(\sigma^y - i\rho^z \sigma^x) & i\Omega(\mathbf{k}, i\omega_n)\rho^z \sigma^z \end{pmatrix}.
\end{aligned} \tag{B14}$$

These results allow us to write down the induced SC action and the pairing functions shown in Eqs. (42) and (43).

Lastly, the RE action for the AF state is given by

$$\begin{aligned}
\delta \tilde{\mathcal{S}}_{\text{RE}} &= \sum_{\mathbf{k}, \omega_n} \sum_{b, b'} [\psi_b^\dagger(\mathbf{k}, i\omega_n) \tilde{\chi}_{bb'}^{\text{RE}}(\mathbf{k}, i\omega_n) \psi_{b'}(\mathbf{k}, i\omega_n) \\
&\quad + \text{H.c.}],
\end{aligned} \tag{B15}$$

where

$$\begin{aligned}
\tilde{\chi}_{\text{AA}}^{\text{RE}}(\mathbf{k}, i\omega_n) &= -\frac{iJ_K^2}{4} \frac{\omega_n(\omega_n^2 + |g(\mathbf{k})|^2 + \lambda^2)\sigma^z}{(\omega_n^2 + \lambda^2)^2 + |g(\mathbf{k})|^2 \omega_n^2}, \\
\tilde{\chi}_{\text{AB}}^{\text{RE}}(\mathbf{k}, i\omega_n) &= \frac{iJ_K^2}{2} \frac{\lambda^2 g(\mathbf{k}) \sigma^-}{(\omega_n^2 + \lambda^2)^2 + |g(\mathbf{k})|^2 \omega_n^2}, \\
\tilde{\chi}_{\text{BA}}^{\text{RE}}(\mathbf{k}, i\omega_n) &= -\frac{iJ_K^2}{2} \frac{\lambda^2 g^*(\mathbf{k}) \sigma^+}{(\omega_n^2 + \lambda^2)^2 + |g(\mathbf{k})|^2 \omega_n^2}, \\
\tilde{\chi}_{\text{BB}}^{\text{RE}}(\mathbf{k}, i\omega_n) &= \frac{iJ_K^2}{4} \frac{\omega_n(\omega_n^2 + |g(\mathbf{k})|^2 + \lambda^2)\sigma^z}{(\omega_n^2 + \lambda^2)^2 + |g(\mathbf{k})|^2 \omega_n^2}.
\end{aligned} \tag{B16}$$

As a result, the above order parameters contain polarization vectors which are no longer restricted to the  $z$  direction.

- 
- [1] P. Anderson, Resonating valence bonds: A new kind of insulator? *Mat. Res. Bull.* **8**, 153 (1973).
  - [2] P. W. Anderson, The Resonating Valence Bond State in  $\text{La}_2\text{CuO}_4$  and Superconductivity, *Science* **235**, 1196 (1987).
  - [3] L. Savary and L. Balents, Quantum spin liquids: a review, *Rep. Prog. Phys.* **80**, 016502 (2016).
  - [4] L. Balents, Spin liquids in frustrated magnets, *Nature (London)* **464**, 199 (2010).
  - [5] X.-G. Wen, Topological orders and edge excitations in fractional quantum Hall states, *Adv. Phys.* **44**, 405 (1995).
  - [6] X.-G. Wen, Quantum orders and symmetric spin liquids, *Phys. Rev. B* **65**, 165113 (2002).
  - [7] A. Kitaev, Anyons in an exactly solved model and beyond, *Ann. Phys. (N. Y.)* **321**, 2 (2006).
  - [8] M. Hermanns, I. Kimchi, and J. Knolle, Physics of the Kitaev model: Fractionalization, dynamic correlations, and material connections, *Annu. Rev. Condens. Matter Phys.* **9**, 17 (2018).
  - [9] S. M. Winter, A. A. Tsirlin, M. Daghofer, J. van den Brink, Y. Singh, P. Gegenwart, and R. Valentí, Models and materials for generalized Kitaev magnetism, *J. Phys.: Condens. Matter* **29**, 493002 (2017).
  - [10] H. Takagi, T. Takayama, G. Jackeli, G. Khaliullin, and S. E. Nagler, Concept and realization of Kitaev quantum spin liquids, *Nat. Rev. Phys.* **1**, 264 (2019).
  - [11] G. Khaliullin, Orbital Order and Fluctuations in Mott Insulators, *Prog. Theor. Phys. Supp.* **160**, 155 (2005).
  - [12] G. Jackeli and G. Khaliullin, Mott Insulators in the strong spin-orbit coupling limit: From Heisenberg to a quantum compass and Kitaev models, *Phys. Rev. Lett.* **102**, 017205 (2009).
  - [13] J. G. Rau, E. K.-H. Lee, and H.-Y. Kee, Generic spin model for the honeycomb iridates beyond the Kitaev limit, *Phys. Rev. Lett.* **112**, 077204 (2014).
  - [14] J. S. Gordon, A. Catuneanu, E. S. Sorensen, and H.-Y. Kee, Theory of the field-revealed Kitaev spin liquid, *Nat. Comm.* **10**, 2041 (2019).
  - [15] G. Chen, R. Pereira, and L. Balents, Exotic phases induced by strong spin-orbit coupling in ordered double perovskites, *Phys. Rev. B* **82**, 174440 (2010).
  - [16] W. M. H. Natori, E. C. Andrade, E. Miranda, and R. G. Pereira, Chiral spin-orbital liquids with nodal lines, *Phys. Rev. Lett.* **117**, 017204 (2016).
  - [17] W. M. H. Natori, M. Daghofer, and R. G. Pereira, Dynamics of a  $j = \frac{3}{2}$  quantum spin liquid, *Phys. Rev. B* **96**, 125109 (2017).
  - [18] J. Romhányi, L. Balents, and G. Jackeli, Spin-orbit dimers and noncollinear phases in  $d^1$  cubic double perovskites, *Phys. Rev. Lett.* **118**, 217202 (2017).
  - [19] F. Wang and A. Vishwanath,  $\text{Z}_2$  spin-orbital liquid state in the square lattice Kugel-Khomskii model, *Phys. Rev. B* **80**, 064413 (2009).
  - [20] W. Witczak-Krempa, G. Chen, Y. B. Kim, and L. Balents, Correlated quantum phenomena in the strong spin-orbit regime, *Annu. Rev. Condens. Matter Phys.* **5**, 57 (2014).



- [21] W. M. H. Natori, E. C. Andrade, and R. G. Pereira, SU(4)-symmetric spin-orbital liquids on the hyperhoneycomb lattice, *Phys. Rev. B* **98**, 195113 (2018).
- [22] M. G. Yamada, M. Oshikawa, and G. Jackeli, Emergent SU(4) symmetry in  $\alpha$ -ZrCl<sub>3</sub> and crystalline spin-orbital liquids, *Phys. Rev. Lett.* **121**, 097201 (2018).
- [23] H. Ishikawa, T. Takayama, R. K. Kremer, J. Nuss, R. Dinnebier, K. Kitagawa, K. Ishii, and H. Takagi, Ordering of hidden multipoles in spin-orbit entangled 5d<sup>1</sup> Ta chlorides, *Phys. Rev. B* **100**, 045142 (2019).
- [24] J. M. Baker, Interactions between ions with orbital angular momentum in insulators, *Rep. Prog. Phys.* **34**, 109 (1971).
- [25] R. Shiina, H. Shiba, and P. Thalmeier, Magnetic-field effects on quadrupolar ordering in a  $\Gamma_8$ -quartet system CeB<sub>6</sub>, *J. Phys. Soc. Jpn.* **66**, 1741 (1997).
- [26] K. Kubo and T. Hotta, Multipole ordering in  $f$ -electron systems on the basis of a  $j$ - $j$  coupling scheme, *Phys. Rev. B* **72**, 144401 (2005).
- [27] P. Santini, S. Carretta, G. Amoretti, R. Caciuffo, N. Magnani, and G. H. Lander, Multipolar interactions in  $f$ -electron systems: The paradigm of actinide dioxides, *Rev. Mod. Phys.* **81**, 807 (2009).
- [28] S. Lee, S. Trebst, Y. B. Kim, and A. Paramekanti, Landau theory of multipolar orders in Pr(Y)<sub>2</sub>X<sub>20</sub> Kondo materials (Y = Ti, V, Rh, Ir; X = Al, Zn), *Phys. Rev. B* **98**, 134447 (2018).
- [29] F.-Y. Li, Y.-D. Li, Y. Yu, A. Paramekanti, and G. Chen, Kitaev materials beyond iridates: Order by quantum disorder and Weyl magnons in rare-earth double perovskites, *Phys. Rev. B* **95**, 085132 (2017).
- [30] S.-H. Jang, R. Sano, Y. Kato, and Y. Motome, Antiferromagnetic Kitaev interaction in  $f$ -electron based honeycomb magnets, *Phys. Rev. B* **99**, 241106(R) (2019).
- [31] J. Xing, E. Feng, Y. Liu, E. Emmanouilidou, C. Hu, J. Liu, D. Graf, A. P. Ramirez, G. Chen, H. Cao, and N. Ni, A Néel-type antiferromagnetic order in the rare-earth Kitaev material candidate YbCl<sub>3</sub>, arXiv e-prints (2019), arXiv:1903.03615.
- [32] A. Koga, H. Tomishige, and J. Nasu, Ground-state and Thermodynamic Properties of an  $S = 1$  Kitaev Model, *J. Phys. Soc. Jpn.* **87**, 063703 (2018).
- [33] J. Oitmaa, A. Koga, and R. R. P. Singh, Incipient and well-developed entropy plateaus in spin- $S$  Kitaev models, *Phys. Rev. B* **98**, 214404 (2018).
- [34] P. P. Stavropoulos, D. Pereira, and H.-Y. Kee, Microscopic mechanism for a higher-spin Kitaev model, *Phys. Rev. Lett.* **123**, 037203 (2019).
- [35] X.-Y. Dong and D. N. Sheng, Spin-1 Kitaev-Heisenberg model on a two-dimensional honeycomb lattice, (2019), arXiv:1911.12854.
- [36] C. Xu, J. Feng, M. Kawamura, Y. Yamaji, Y. Nahas, S. Prokhorenko, Y. Qi, H. Xiang, and L. Bellaiche, Possible Kitaev Quantum Spin Liquid State in 2D Materials with  $S = 3/2$ , *Phys. Rev. Lett.* **124**, 087205 (2020).
- [37] C. Hickey, C. Berke, P. P. Stavropoulos, H.-Y. Kee, and S. Trebst, Field-driven gapless spin liquid in the spin-1 Kitaev honeycomb model, (2020), arXiv:2001.07699.
- [38] H. Yao, S.-C. Zhang, and S. A. Kivelson, Algebraic Spin Liquid in an Exactly Solvable Spin Model, *Phys. Rev. Lett.* **102**, 217202 (2009).
- [39] C. Wu, D. Arovas, and H.-H. Hung,  $\Gamma$ -matrix generalization of the Kitaev model, *Phys. Rev. B* **79**, 134427 (2009).
- [40] H. Yao and D.-H. Lee, Fermionic magnons, non-abelian spinons, and the spin quantum Hall effect from an exactly solvable spin-1/2 Kitaev model with SU(2) symmetry, *Phys. Rev. Lett.* **107**, 087205 (2011).
- [41] V. Dwivedi, C. Hickey, T. Eschmann, and S. Trebst, Majorana corner modes in a second-order Kitaev spin liquid, *Phys. Rev. B* **98**, 054432 (2018).
- [42] Z. Nussinov and J. van den Brink, Compass models: Theory and physical motivations, *Rev. Mod. Phys.* **87**, 1 (2015).
- [43] A. Abragam and B. Bleaney, *Electron Paramagnetic Resonance of Transition Ions*, International series of monographs on physics (OUP Oxford, 2012).
- [44] U. F. P. Seifert, T. Meng, and M. Vojta, Fractionalized Fermi liquids and exotic superconductivity in the Kitaev-Kondo lattice, *Phys. Rev. B* **97**, 085118 (2018).
- [45] W. Choi, P. W. Klein, A. Rosch, and Y. B. Kim, Topological superconductivity in the Kondo-Kitaev model, *Phys. Rev. B* **98**, 155123 (2018).
- [46] S. Biswas, Y. Li, S. M. Winter, J. Knolle, and R. Valentí, Electronic properties of  $\alpha$ -RuCl<sub>3</sub> in proximity to graphene, *Phys. Rev. Lett.* **123**, 237201 (2019).
- [47] G. Zhang, J. S. Van Dyke, and R. Flint, Cubic hysteric order in the two-channel Kondo-Heisenberg model, *Phys. Rev. B* **98**, 235143 (2018).
- [48] A. S. Patri, I. Khait, and Y. B. Kim, Emergent non-Fermi-liquid phenomena in multipolar quantum impurity systems, *Phys. Rev. Research* **2**, 013257 (2020).
- [49] V. Berezinskii, New model of the anisotropic phase of superfluid <sup>3</sup>He, *JETP Lett.* **20**, 287 (1974).
- [50] A. Balatsky and E. Abrahams, New class of singlet superconductors which break the time reversal and parity, *Phys. Rev. B* **45**, 13125 (1992).
- [51] P. Coleman, E. Miranda, and A. Tsvelik, Possible realization of odd-frequency pairing in heavy fermion compounds, *Phys. Rev. Lett.* **70**, 2960 (1993).
- [52] P. Coleman, E. Miranda, and A. Tsvelik, Odd-frequency pairing in the Kondo lattice, *Phys. Rev. B* **49**, 8955 (1994).
- [53] J. Linder and A. V. Balatsky, Odd-frequency superconductivity, *Rev. Mod. Phys.* **91**, 045005 (2019).
- [54] P. M. R. Brydon, D. F. Agterberg, H. Menke, and C. Timm, Bogoliubov Fermi surfaces: General theory, magnetic order, and topology, *Phys. Rev. B* **98**, 224509 (2018).
- [55] E. Colomés and M. Franz, Antichiral Edge States in a Modified Haldane Nanoribbon, *Phys. Rev. Lett.* **120**, 086603 (2018).
- [56] D. H. McMahon and R. H. Silsbee, Virtual phonon effects in the paramagnetic resonance of MgO:Fe<sup>++</sup>, *Phys. Rev.* **135**, A91 (1964).
- [57] G. Khaliullin and S. Okamoto, Quantum behavior of orbitals in ferromagnetic titanates: Novel orderings and excitations, *Phys. Rev. Lett.* **89**, 167201 (2002).
- [58] E. H. Lieb, Flux phase of the half-filled band, *Phys. Rev. Lett.* **73**, 2158 (1994).
- [59] V. J. Emery and S. Kivelson, Mapping of the two-channel kondo problem to a resonant-level model, *Phys. Rev. B* **46**, 10812 (1992).
- [60] V. J. Emery and S. A. Kivelson, Solution of an orbital Kondo array, *Phys. Rev. Lett.* **71**, 3701 (1993).
- [61] E. Abrahams, A. Balatsky, D. J. Scalapino, and J. R. Schrieffer, Properties of odd-gap superconductors, *Phys. Rev. B* **52**, 1271 (1995).

- [62] O. Zachar, S. A. Kivelson, and V. J. Emery, Exact Results for a 1D Kondo Lattice from Bosonization, *Phys. Rev. Lett.* **77**, 1342 (1996).
- [63] J. Linder and A. V. Balatsky, Odd-frequency superconductivity, *Rev. Mod. Phys.* **91**, 045005 (2019).
- [64] R. M. Fernandes, P. P. Orth, and J. Schmalian, Intertwined vestigial order in quantum materials: Nematicity and beyond, *Annu. Rev. Condens. Matter Phys.* **10**, 133 (2019).
- [65] O. Erten, P.-Y. Chang, P. Coleman, and A. M. Tsvelik, Skyrme insulators: Insulators at the brink of superconductivity, *Phys. Rev. Lett.* **119**, 057603 (2017).
- [66] T. H. Hsieh, H. Ishizuka, L. Balents, and T. L. Hughes, Bulk Topological Proximity Effect, *Phys. Rev. Lett.* **116**, 086802 (2016).
- [67] T. H. Hsieh, Y.-M. Lu, and A. W. W. Ludwig, Topological bootstrap: Fractionalization from Kondo coupling, *Sci. Adv.* **3**, e1700729 (2017).
- [68] J. A. Krieger, A. Pertsova, S. R. Giblin, M. Döbeli, T. Prokscha, C. W. Schneider, A. Suter, T. Hesjedal, A. V. Balatsky, and Z. Salman, Proximity-induced odd-frequency superconductivity in a topological insulator, (2020), [arXiv:2003.12104](#).
- [69] Y. Cao, V. Fatemi, S. Fang, K. Watanabe, T. Taniguchi, E. Kaxiras, and P. Jarillo-Herrero, Unconventional superconductivity in magic-angle graphene superlattices, *Nature (London)* **556** (2018).
- [70] H. C. Po, L. Zou, A. Vishwanath, and T. Senthil, Origin of Mott insulating behavior and superconductivity in twisted bilayer graphene, *Phys. Rev. X* **8**, 031089 (2018).
- [71] K. S. Novoselov, A. Mishchenko, A. Carvalho, and A. H. Castro Neto, 2D materials and van der Waals heterostructures, *Science* **353** (2016).